A&A 511, A16 (2010)
DOI: 10.1051/0004-6361/200913574

Astronomy & Astrophysics

Transition probabilities of astrophysical interest in the niobium ions Nb^+ and Nb^{2+}

H. Nilsson[1], H. Hartman[1], L. Engström[2], H. Lundberg[2], C. Sneden[3], V. Fivet[4], P. Palmeri[4], P. Quinet[4,5], and É. Biémont[4,5]

[1] Lund Observatory, Lund University, Box 43, 221 00 Lund, Sweden
e-mail: hampus.nilsson@astro.lu.se
[2] Department of Physics, Lund University, Box 118, 221 00 Lund, Sweden
[3] Department of Astronomy, University of Texas, RLM 15.308, Austin TX78712, USA
[4] Astrophysique et Spectroscopie, Université de Mons, 20 Place du Parc, 7000 Mons, Belgium
[5] IPNAS, Bât. B15, Université de Liège, Sart Tilman, 4000 Liège, Belgium

Received 29 October 2009 / Accepted 20 November 2009

ABSTRACT

Aims. We attempt to derive accurate transition probabilities for astrophysically interesting spectral lines of Nb II and Nb III and determine the niobium abundance in the Sun and metal-poor stars rich in neutron-capture elements.
Methods. We used the time-resolved laser-induced fluorescence technique to measure radiative lifetimes in Nb II. Branching fractions were measured from spectra recorded using Fourier transform spectroscopy. The radiative lifetimes and the branching fractions were combined yielding transition probabilities. In addition, we calculated lifetimes and transition probablities in Nb II and Nb III using a relativistic Hartree-Fock method that includes core polarization. Abundances of the sun and five metal-poor stars were derived using synthetic spectra calculated with the MOOG code, including hyperfine broadening of the lines.
Results. We present laboratory measurements of 17 radiative lifetimes in Nb II. By combining these lifetimes with branching fractions for lines depopulating the levels, we derive the transition probabilities of 107 Nb II lines from $4d^3 5p$ configuration in the wavelength region 2240−4700 Å. For the first time, we present theoretical transition probabilities of 76 Nb III transitions with wavelengths in the range 1430−3140 Å. The derived solar photospheric niobium abundance $\log \epsilon_\odot = 1.44 \pm 0.06$ is in agreement with the meteoritic value. The stellar Nb/Eu abundance ratio determined for five metal-poor stars confirms that the *r*-process is a dominant production method for the *n*-capture elements in these stars.

Key words. atomic data – atomic processes – Sun: abundances – stars: abundances

1. Introduction

About half of the stable nuclei heavier than iron are believed to be synthesized by means of a slow neutron-capture process (the "*s*-process") in the late stages of the evolution of stars with masses in the range 0.8−8 $M_{\rm Sun}$. This process occurs when the star is in the "asymptotic giant branch" (AGB) phase of its life. During this phase, the star experiences a series of thermal pulses, which consist of recurrent thermal instabilities that lead to rich nucleosynthesis by means of the *s*-process. After each thermal pulse, the deep convective envelope of the star penetrates the region where *s*-process elements have been produced and brings them to the stellar surface, where they become observable (see e.g., Lugaro et al. 2003).

The *s*-process elements technetium, niobium, and ruthenium are particularly interesting because they give information about the timescales involved in addition providing insight into the *s*-process. Niobium is not produced directly by the *s*-process (unless the neutron density is extremely low), and the niobium abundance is probably dominated by ^{93}Nb from the decay of ^{93}Zr (generated by the *s*-process) with a lifetime of about 1.5×10^6 years (see e.g., Allen & Porto de Mello 2007).

The abundance of technetium, niobium, and ruthenium are important for constraining evolutionary lifetimes during the thermally-pulsing AGB phase. However, only one study was devoted to the time evolution of these elements in stars. Wallerstein & Dominy (1988) investigated the technetium, niobium, and zirconium abundances in a sample of AGB M and MS stars and derived timescales of the shell flashes. The abundances were derived from equivalent width measurements (which are sensitive to line blends) using the log gf values of Duquette et al. (1986) for Nb I and the f-values of Garstang (1981) for Tc I.

Technetium, niobium, and ruthenium studies are relatively uncommon simply because it is difficult to derive accurate abundances of these elements. Their available transitions are few in number and mostly weak and/or blended. Fortunately, sophisticated model atmospheres and synthetic spectrum techniques are now available for deriving reliable abundances from a small number of transitions. A few studies have been devoted to technetium abundance determinations (e.g., Van Eck & Jorissen 1999; Lebzelter & Hron 1999; Vanture et al. 2007). In this paper, we derive accurate niobium abundances for the Sun and several very metal-poor stars with enhanced neutron-capture abundances.

Lifetimes in Nb II were reported by Salih & Lawler (1983), which were measured using time-resolved laser-induced fluorescence (TR-LIF) on a Nb^+ beam. Hannaford et al. (1985) measured 27 lifetimes for low-lying $5d^3 5p$ energy levels using TR-LIF and a sputtered metal vapor. In addition, they

derived transition probabilities by using the branching fractions taken from Corliss & Bozman (1962), and used them to determine the solar abundance of niobium. Transition probabilities for 145 lines in Nb II were reported by Nilsson & Ivarsson (2008), who measured branching fractions (*BF*s) in the wavelength interval 2600−4600 Å. In addition, Nilsson & Ivarsson (2008) combined the *BF*s with the lifetimes from Hannaford et al. (1985) to obtain transition probabilities for the 145 lines. Nilsson & Ivarsson (2008) also reported hyperfine splitting constants for 28 even and 24 odd levels. The present paper is a continuation of the work reported by Nilsson & Ivarsson (2008).

The only previous theoretical work on Nb II was that of Beck & Datta (1995), who used a relativistic configuration-interaction (RCI) method to compute f-values for transitions connecting the $J = 2, 3, 4$ $(4d+5s)^4$ states to the $4d^3(^4F)5p\ ^5G^\circ_3$ and $^3D^\circ_3$ levels. To our knowledge, there are no transition probabilities or radiative lifetimes available for Nb^{2+} in the literature.

In the present work, we report f-values of 107 Nb II transitions in the spectral range 2242−4700 Å. In addition, a first set of 76 astrophysically interesting transition probabilities in Nb III are calculated using a theoretical model similar to that used in Nb II.

2. Measurements of lifetimes and branching fractions

Transition probabilities can be measured in several ways (see Huber & Sandeman 1986, for a review). We used the emission technique, where radiative lifetimes measured with TR-LIF are combined with *BF*s derived from spectra recorded using Fourier transform spectroscopy (FTS). With this technique, it is possible to obtain a large amount of accurate transition probabilities over a wide wavelength range.

The lifetime of an upper state u can be written as

$$\tau_u = 1/\sum_k A_{uk}, \tag{1}$$

and the BF of a line, from the upper state u to a lower state l, is defined as

$$BF_{ul} = A_{ul}/\sum_k A_{uk}. \tag{2}$$

Combining these two equations provides us with the transition probabilities

$$A_{ul} = BF_{ul}/\tau_u. \tag{3}$$

In the following sections, the experimental measurements of the radiative lifetimes and *BF*s are described.

2.1. Radiative lifetimes

We report the experimental lifetimes of 17 short-lived, odd-parity levels in Nb II belonging to the $4d^35p$ configuration. The measurements were performed using TR-LIF on ions in a laser-produced plasma. The TR-LIF technique previously provided accurate lifetimes in many different systems (see Fivet et al. 2006, 2008). A detailed description of the experimental setup is reported in Bergstöm et al. (1988) and Xu et al. (2003, 2004) and only a brief description is presented in this paper.

Niobium ions in different excited states were generated in a laser-produced plasma obtained by focusing a 5320 Å Nd:YAG laser pulse (Continuum Surelite) onto a rotating niobium target. The different ionization stages have different velocities and can be separated by selecting an appropriate delay time between the ablation and the excitation pulses.

Excitation pulses, with a duration of 1−2 ns, were obtained from a frequency-doubled Nd:YAG laser (Continuum NY-82) temporally compressed in a stimulated Brillouin scattering cell. To generate the required excitation wavelengths, the compressed pulses were used to pump a dye laser (Continuum Nd-60). Excitation wavelengths as low as 1910 Å can be obtained using the DCM dye and non-linear processes, such as frequency doubling and tripling in KDP and BBO crystals and stimulated Raman scattering in a hydrogen gas cell.

The excitation beam interacted with the niobium ions about 1 cm above the target. The fluorescence emitted from the excited levels was focused with a fused-silica lens onto the entrance slit of a 1/8 m monochromator, and detected by a Hamamatsu R3809U micro-channel-plate photomultiplier tube with a risetime of 0.15 ns. The fluorescence signal was recorded by a transient digitizer with a time resolution of 0.5 ns. The temporal shape of the laser pulse was recorded simultaneously with a fast diode. Each decay curve was typically averaged over 1000 laser pulses.

The computer code DECFIT was developed to analyze the fluorescence signals. DECFIT operates on a Windows platform and provides the user with an efficient graphical environment. Lifetimes are extracted using a weighted least squares fit to a single exponential decay convolved with the shape of the laser pulse to the fluorescence signal. In addition, a polynomial background representation can be added in the fit.

The new experimental lifetimes for 17 levels in Nb II are reported in Table 1. The lifetimes are averages from at least ten recordings. The error estimates take into account the statistical uncertainties in the fitting as well as variations between the different recordings. The results reported by Salih & Lawler (1983) and by Hannaford et al. (1985) are shown for comparison as well as the theoretical data obtained by Beck & Datta (1995).

2.2. Branching fractions

The intensity of a spectral line is dependent on the population (N_u), the transition probability (A_{uk}), and the statistical weight (g_u) of the upper level. The BF can therefore be derived by measuring the intensities of all lines from a given upper level u

$$BF_{ul} = A_{ul}/\sum_k A_{uk} = I_{ul}/\sum_k I_{uk}, \tag{4}$$

where I_{ul} is the intensity of a line from upper level u to lower level l corrected for the wavenumber dependent efficiency of the detection system. One advantage of this method is that neither the population of the upper level u nor the population mechanisms have to be known.

The intensities were measured with FTS. Spectra between 20 000 and 50 000 cm^{-1} (5000−2000 Å) were recorded with the Lund UV Chelsea Instruments FT spectrometer. A custom-built hollow cathode discharge lamp (HCDL) was used to produce the Nb^+ ions. The HCDL was operated with a mixture of argon and neon as carrier gases at 1−2 Torr. Two different detectors were used. Between 20 000 and 40 000 cm^{-1}, we used a Hamamatsu R955 PM tube, whereas the 30 000 to 50 000 cm^{-1} region was recorded with a solar blind Hamamatsu R166 PM tube. The first region was intensity-calibrated using known

Table 1. Calculated and experimental lifetimes for Nb II levels of the $4d^3 5p$ configuration.

Desig.[a]	E^a (cm^{-1})	Theory τ(ns) HFR(A) this work	Theory τ(ns) HFR(B) this work	τ(ns) previous	Experiment τ(ns) this work	τ(ns) previous
$4d^3(^4F)5p\ ^5G^\circ_2$	33 351.09	5.0	5.6			5.9(4)[e]
$4d^3(^4F)5p\ ^5G^\circ_3$	33 919.24	4.9	5.5	5.16[b] , 6.53[c]		6.2(3)[d] , 5.8(3)[e]
$4d^3(^4F)5p\ ^5G^\circ_4$	34 632.03	4.7	5.3			5.8(3)[d] , 5.5(3)[e]
$4d^3(^4F)5p\ ^3D^\circ_1$	34 886.35	5.1	5.9		5.6(3)	5.5(3)[d] , 5.7(3)[e]
$4d^3(^4F)5p\ ^5G^\circ_5$	35 474.20	4.6	5.2			5.3(3)[d] , 5.3(3)[e]
$4d^3(^4F)5p\ ^3D^\circ_2$	35 520.82	4.8	5.7		5.5(3)	5.7(3)[d] , 5.7(3)[e]
$4d^3(^4F)5p\ ^5G^\circ_6$	36 455.46	4.4	5.0			5.0(3)[d] , 5.1(3)[e]
$4d^3(^4F)5p\ ^3D^\circ_3$	36 553.24	4.2	5.0	4.67[b] , 5.60[c]		5.0(3)[d] , 5.0(3)[e]
$4d^3(^4F)5p\ ^5F^\circ_1$	36 731.81	4.0	4.7			4.7(3)[e]
$4d^3(^4F)5p\ ^5F^\circ_2$	36 962.77	4.0	4.7			4.7(3)[e]
$4d^3(^4F)5p\ ^5D^\circ_0$	37 298.24	2.3	2.7		2.6(2)	3.1(3)[e]
$4d^3(^4F)5p\ ^5F^\circ_3$	37 376.90	3.9	4.6			4.7(3)[e]
$4d^3(^4F)5p\ ^5D^\circ_1$	37 480.08	2.4	2.7			3.1(3)[e]
$4d^3(^4F)5p\ ^5F^\circ_4$	37 528.38	3.8	4.4			4.6(3)[e]
$4d^3(^4F)5p\ ^5D^\circ_2$	37 797.32	2.6	2.8		2.7(2)	3.2(3)[e]
$4d^3(^4F)5p\ ^5F^\circ_5$	38 024.34	3.9	4.6			4.6(3)[e]
$4d^3(^4F)5p\ ^5D^\circ_3$	38 216.39	2.7	3.0			3.4(3)[e]
$4d^3(^4F)5p\ ^5D^\circ_4$	38 291.25	2.6	3.0			3.3(3)[e]
$4d^3(^4F)5p\ ^3G^\circ_3$	38 684.96	4.5	5.1			5.0(3)[e]
$4d^3(^4F)5p\ ^3F^\circ_2$	38 984.39	6.8	7.3			7.3(3)[e]
$4d^3(^4F)5p\ ^3G^\circ_4$	39 335.27	4.5	5.1			5.1(3)[e]
$4d^3(^4F)5p\ ^3F^\circ_3$	39 779.92	6.3	6.9			6.8(3)[e]
$4d^3(^4F)5p\ ^3G^\circ_5$	40 103.61	4.4	5.0		5.1(3)	5.2(3)[e]
$4d^3(^4F)5p\ ^3F^\circ_4$	40 561.02	5.8	6.3			6.4(3)[e]
$4d^3(^4P)5p\ ^3P^\circ_2$	41 710.14	7.9	8.4		8.5(7)	
$4d^3(^4P)5p\ ^3P^\circ_1$	42 132.65	6.5	7.2		7.2(5)	
$4d^3(^4P)5p\ ^5D^\circ_0$	42 596.55	6.3	7.2		7.5(7)	
$4d^3(^4P)5p\ ^5D^\circ_2$	43 290.34	6.9	7.3		7.5(4)	
$4d^3(^2P)5p\ ^1D^\circ_2$	43 618.39	6.4	6.7		6.7(3)	
$4d^3(^2P)5p\ ^3D^\circ_1$	43 649.19	8.4	8.1		7.2(4)	12.8(3)[e]
$4d^3(^4P)5p\ ^5D^\circ_3$	43 887.08	5.9	6.3		5.7(5)	
$4d^3(^4P)5p\ ^5D^\circ_1$	44 066.67	5.8	6.7		6.4(5)	5.3(3)[e]
$4d^3(^4P)5p\ ^3P^\circ_0$	44 285.94	6.6	7.5		7.0(5)	
$4d^3(^2P)5p\ ^3D^\circ_2$	44 924.60	5.9	6.6		6.2(3)	
$4d^3(^4P)5p\ ^5D^\circ_4$	44 970.71	5.1	5.8		5.2(5)	
$4d^3(^2P)5p\ ^3D^\circ_3$	45 802.47	4.9	4.6		4.6(3)	
$4d^3(^2H)5p\ ^3H^\circ_6$	48 770.84	4.5	3.7			4.2(3)[e]

Notes. [(a)] From Ryabtsev et al. (2000); [(b)] from Beck & Datta (1995): length form; [(c)] from Beck & Datta (1995): velocity form; [(d)] from Salih & Lawler (1983); [(e)] from Hannaford et al. (1985). $A(B)$ is written for $A \pm B$.

branching ratios in argon (Whaling et al. 1993), while the UV spectra were intensity-calibrated with a deuterium lamp, itself calibrated at the Physikalisch-Technische Bundesanstalt (PTB), Berlin, Germany.

The lines were checked for possible effects of self-absorption by recording several spectra at different HCDL currents thus changing the populations of the different levels.

In Table 2, we list all *BF*s measured in this work as well as the theoretical values (see next section). The results are compared with theoretical *BF*s calculated within the framework of the HFR+CPOL approach. The lines are sorted by upper level. The level designation and energies are from Ryabtsev et al. (2000). The uncertainties given in Col. 10 are calculated according to the method suggested by Sikström et al. (2002). In addition, we list the transition probabilities and the oscillator strengths deduced from the experimental lifetimes as well as the measured branching fractions.

Not all transitions are strong enough to be seen in the spectra recorded by the HCDL, but the sum of all these unmeasurable weak transitions, the residuals, can be estimated with theoretical calculations. The differences between the experimental and the theoretical *BF*s are shown in Fig. 1. The signal-to-noise ratio of a line affected by hyperfine structure is lower because the intensity of the line is distributed between the different components. This is a problem for weak transitions. In addition, the theoretical *BF*s of the weakest transitions are more difficult to calculate accurately than those of the strongest lines because they are sensitive to small configuration interaction effects and to possible cancellation effects in the line strengths. This explains the larger scatter in the left part of Fig. 1.

Table 2. Experimental branching fractions (BF), A-values, and gf-values in Nb II. $A(B)$ is written for $A \times 10^B$.

Upper level	Lower level	λ_{air}	σ	BF			A	log (gf)	Unc.
	Design.	(Å)	(cm^{-1})	Calc.	Exp.	Exp/Calc	(s^{-1})		(% in gf)
$4d^3(^4F)5p\ ^3F^\circ_4$	$4d^4\ ^5D_3$	2514.3531	39 759.692	0.012	0.013	1.089	2.06(6)	–1.76	13
	$4d^4\ ^5D_4$	2541.4244	39 336.195	0.067	0.069	1.033	1.09(7)	–1.02	12
40561.02 cm^{-1}	$4d^3(^4F)5s\ ^5F_4$	2700.5523	37 018.457	0.026	0.035	1.336	5.47(6)	–1.27	12
	$4d^3(^4F)5s\ ^5F_5$	2745.3118	36 414.981	0.079	0.086	1.087	1.35(7)	–0.86	12
	$4d^4\ ^3F_4$	3100.7738	32 240.645	0.025	0.025	0.984	3.88(6)	–1.30	17
	$4d^4\ ^3G_5$	3372.5601	29 642.544	0.055	0.065	1.197	1.02(7)	–0.80	8
	$4d^3(^4P)5s\ ^5P_3$	3421.1646	29 221.428	0.015	0.018	1.158	2.77(6)	–1.36	12
	$4d^3(^4F)5s\ ^3F_4$	3717.0600	26 895.332	0.348	0.368	1.055	5.75(7)	0.03	8
	$4d^3(^4F)5s\ ^3F_3$	3720.4532	26 870.790	0.080	0.105	1.304	1.64(7)	–0.51	8
	$4d^4\ ^1G_4$	3879.3421	25 770.263	0.171	0.089	0.523	1.40(7)	–0.55	6
	$4d^3(^2G)5s\ ^3G_4$	4061.9711	24 611.648	0.021	0.027	1.274	4.27(6)	–1.02	9
	Residual				0.099				
$4d^3(^4P)5p\ ^3P^\circ_2$	$4d^4\ ^3F_3$	2956.8884	33 809.499	0.061	0.065	1.073	7.89(6)	–1.29	21
	$4d^3(^4P)5s\ ^5P_2$	3237.9954	30 874.306	0.248	0.199	0.802	2.42(7)	–0.72	11
41710.14 cm^{-1}	$4d^4\ ^1D_2$	3394.9714	29 446.922	0.151	0.153	1.008	1.85(7)	–0.80	11
	$4d^3(^4F)5s\ ^3F_2$	3541.2454	28 230.683	0.099	0.124	1.244	1.50(7)	–0.85	11
	$4d^3(^2P)5s\ ^3P_1$	3691.1738	27 083.944	0.071	0.073	1.040	5.60(6)	–1.24	14
	$4d^3(^2P)5s\ ^3P_2$	3695.8960	27 049.388	0.183	0.193	1.057	2.35(7)	–0.62	11
	$4d^3(^2D2)5s\ ^3D_1$	4367.3789	22 890.623	0.035	0.037	1.041	4.48(6)	–1.19	16
	$4d^3(^4P)5s\ ^3P_1$	4699.5812	21 272.640	0.041	0.046	1.110	5.53(6)	–1.04	19
	Residual				0.110				
$4d^3(^4P)5p\ ^3P^\circ_1$	$4d^4\ ^5D_0$	2372.7316	42 132.646	0.024	0.014	0.598	1.93(6)	–2.31	22
	$4d^4\ ^5D_1$	2381.7200	41 973.662	0.026	0.018	0.690	2.37(6)	–2.22	18
42132.65 cm^{-1}	$4d^4\ ^3P_2$	2866.8425	34 871.322	0.038	0.015	0.403	2.03(6)	–2.13	52
	$4d^4\ ^3F_2$	2887.0836	34 626.881	0.042	0.060	1.426	8.00(6)	–1.52	21
	$4d^3(^4P)5s\ ^5P_1$	3175.7747	31 479.219	0.263	0.273	1.038	3.64(7)	–0.78	11
	$4d^3(^4P)5s\ ^5P_2$	3194.2782	31 296.809	0.259	0.281	1.083	3.75(7)	–0.77	11
	$4d^3(^2P)5s\ ^3P_2$	3639.0501	27 471.891	0.132	0.131	0.990	1.75(7)	–0.98	12
	$4d^3(^2P)5s\ ^3P_0$	3641.3782	27 454.328	0.037	0.034	0.936	4.59(6)	–1.56	20
	$4d^3(^4P)5s\ ^3P_0$	4588.9970	21 785.149	0.033	0.028	0.836	3.67(6)	–1.46	23
	Residual				0.146				
$4d^3(^4P)5p\ ^3P^\circ_0$	$4d^4\ ^5D_1$	2265.4874	44 126.956	0.025	0.04	1.612	5.66(5)	–2.36	28
44285.94 cm^{-1}	$4d^4\ ^3P_1$	2624.3286	38 093.630	0.003	0.10	31.295	1.41(6)	–1.84	21
	$4d^3(^4P)5s\ ^5P_1$	2972.4398	33 632.513	0.246	0.14	0.558	1.96(6)	–1.59	47
	$4d^3(^2P)5s\ ^3P_1$	3370.6053	29 659.741	0.601	0.60	0.997	8.56(6)	–0.84	13
	Residual				0.120				
$4d^3(^4P)5p\ ^5D^\circ_0$	$4d^3(^4P)5s\ ^5P_1$	3129.6522	31 943.127	0.756	0.756	1.000	1.05(8)	–0.814	12
42596.55 cm^{-1}	*Residual*				0.244				
$4d^3(^4P)5p\ ^5D^\circ_2$	$4d^4\ ^5D_2$	2332.8990	42 851.977	0.029	0.021	0.731	2.86(6)	–1.93	21
	$4d^4\ ^3F_2$	2793.6766	35 784.573	0.029	0.047	1.649	6.30(6)	–1.43	19
43290.34 cm^{-1}	$4d^3(^4P)5s\ ^5P_1$	3063.1193	32 636.911	0.120	0.132	1.103	1.76(7)	–0.91	14
	$4d^3(^4P)5s\ ^5P_2$	3080.3475	32 454.501	0.309	0.346	1.120	4.62(7)	–0.48	10
	$4d^3(^4P)5s\ ^5P_3$	3128.9145	31 950.748	0.054	0.047	0.855	6.21(6)	–1.34	22
	$4d^4\ ^1D_2$	3222.0580	31 027.117	0.226	0.178	0.789	2.38(7)	–0.73	12
	$4d^3(^2D2)5s\ ^3D_1$	4085.3468	24 470.818	0.030	0.031	1.034	4.16(6)	–1.28	18
	$4d^3(^2P)5s\ ^1P_1$	4492.9563	22 250.809	0.072	0.066	0.921	8.83(6)	–0.87	14
	Residual				0.130				
$4d^3(^2P)5p\ ^1D^\circ_2$	$4d^4\ ^5D_1$	2300.2897	43 459.407	0.019	0.013	0.685	1.93(6)	–2.12	15
	$4d^4\ ^5D_2$	2315.1745	43 180.030	0.062	0.040	0.639	5.81(6)	–1.63	11
43618.39 cm^{-1}	$4d^4\ ^5D_3$	2334.8014	42 817.065	0.037	0.030	0.820	4.40(6)	–1.75	14
	$4d^4\ ^3P_2$	2749.6848	36 357.067	0.044	0.057	1.299	8.37(6)	–1.32	12
	$4d^4\ ^3F_3$	2798.9044	35 717.747	0.063	0.108	1.704	1.58(7)	–1.03	11
	$4d^3(^4P)5s\ ^5P_1$	3032.6351	32 964.964	0.021	0.054	2.615	7.96(6)	–1.26	19
	$4d^3(^4P)5s\ ^5P_2$	3049.5039	32 782.554	0.038	0.066	1.767	1.30(7)	–1.04	13
	$4d^3(^4P)5s\ ^5P_3$	3097.1160	32 278.801	0.192	0.138	0.719	2.03(7)	–0.84	11
	$4d^4\ ^1D_2$	3188.3466	31 355.170	0.034	0.023	0.685	3.40(6)	–1.59	30
	$4d^4\ ^3D_2$	3244.5078	30 812.426	0.047	0.048	1.030	7.02(6)	–1.26	15
	$4d^4\ ^3D_1$	3277.7583	30 499.863	0.020	0.019	0.918	2.72(6)	–1.66	32
	$4d^3(^4F)5s\ ^3F_3$	3340.3740	29 928.163	0.018	0.021	1.170	3.11(6)	–1.59	26
	$4d^3(^2P)5s\ ^3P_1$	3448.2179	28 992.192	0.083	0.067	0.814	9.86(6)	–1.06	14

Table 2. continued.

Upper level	Lower level Design.	λ_{air} (Å)	σ (cm^{-1})	Calc.	*BF* Exp.	Exp/Calc	*A* (s^{-1})	log (*gf*)	Unc. (% in *gf*)
	$4d^3(^2P)5s\ ^3P_2$	3452.3409	28 957.636	0.162	0.153	0.946	2.24(7)	–0.70	11
	$4d^3(^4P)5s\ ^3P_2$	4522.1931	22 107.015	0.027	0.028	1.029	4.12(6)	–1.20	20
	Residual				0.133				
$4d^3(^2P)5p\ ^3D^\circ_1$	$4d^4\ ^3P_2$	2747.3562	36 387.869	0.102	0.249	2.431	3.40(7)	–0.94	10
	$4d^4\ ^3F_2$	2765.9299	36 143.428	0.186	0.076	0.409	1.04(7)	–1.45	12
43649.19 cm^{-1}	$4d^3(^4P)5s\ ^5P_1$	3029.8088	32 995.766	0.028	0.138	4.942	1.88(7)	–1.11	11
	$4d^3(^2P)5s\ ^3P_2$	3448.6696	28 988.438	0.095	0.073	0.770	1.51(7)	–1.09	12
	$4d^3(^2P)5s\ ^3P_0$	3450.7619	28 970.875	0.301	0.178	0.590	2.36(7)	–0.90	10
	$4d^3(^2D2)5s\ ^3D_1$	4026.3014	24 829.673	0.046	0.049	1.063	4.09(6)	–1.53	23
	$4d^3(^2D2)5s\ ^3D_2$	4114.5320	24 297.245	0.046	0.035	0.752	4.77(6)	–1.44	21
	$4d^3(^2P)5s\ ^1P_1$	4421.6458	22 609.664	0.034	0.041	1.224	5.62(6)	–1.31	29
	Residual				0.162				
$4d^3(^4P)5p\ ^5D^\circ_3$	$4d^4\ ^5D_2$	2300.8551	43 448.717	0.015	0.012	0.780	1.98(6)	–1.96	21
	$4d^4\ ^5D_3$	2320.2400	43 085.752	0.033	0.028	0.834	4.73(6)	–1.57	16
43887.08 cm^{-1}	$4d^4\ ^5D_4$	2343.2745	42 662.255	0.010	0.012	1.220	2.09(6)	–1.92	29
	$4d^4\ ^3P_2$	2729.5123	36 625.754	0.014	0.013	0.925	2.20(6)	–1.77	24
	$4d^4\ ^3F_4$	2810.7918	35 566.705	0.088	0.122	1.384	2.48(7)	–0.69	15
	$4d^3(^4P)5s\ ^5P_2$	3024.7316	33 051.241	0.477	0.401	0.841	6.86(7)	–0.18	15
	$4d^3(^4P)5s\ ^5P_3$	3071.5463	32 547.488	0.262	0.305	1.165	5.23(7)	–0.29	15
	$4d^4\ ^3D_3$	3242.4077	30 832.382	0.011	0.018	1.656	3.08(6)	–1.47	49
	$4d^3(^4P)5s\ ^3P_2$	4467.8849	22 375.702	0.016	0.015	0.949	2.62(6)	–1.26	22
	Residual				0.074				
$4d^3(^4P)5p\ ^5D^\circ_1$	$4d^4\ ^5D_2$	2291.3844	43 628.304	0.023	0.014	0.609	2.18(6)	–2.29	26
	$4d^4\ ^3F_2$	2734.3521	36 560.900	0.083	0.124	1.487	1.94(7)	–1.19	17
44066.67 cm^{-1}	$4d^3(^4P)5s\ ^5P_1$	2991.9493	33 413.238	0.379	0.276	0.727	4.31(7)	–0.76	19
	$4d^3(^2P)5s\ ^3P_1$	3395.7224	29 440.466	0.131	0.065	0.498	1.02(7)	–1.28	22
	$4d^3(^2P)5s\ ^3P_2$	3399.7112	29 405.910	0.154	0.291	1.894	4.55(7)	–0.63	17
	Residual				0.230				
$4d^3(^2P)5p\ ^3D^\circ_2$	$4d^4\ ^5D_3$	2265.6748	44 123.277	0.059	0.072	1.217	1.10(7)	–1.37	13
	$4d^4\ ^3F_2$	2671.6567	37 418.838	0.028	0.016	0.582	9.32(6)	–1.30	14
44924.60 cm^{-1}	$4d^4\ ^3F_3$	2700.1527	37 023.959	0.211	0.250	1.187	3.82(7)	–0.68	12
	$4d^3(^4P)5s\ ^5P_1$	2917.0516	34 271.176	0.186	0.225	1.206	3.43(7)	–0.66	13
	$4d^3(^4F)5s\ ^3F_2$	3179.2265	31 445.143	0.021	0.025	1.200	3.86(6)	–1.53	65
	$4d^3(^2P)5s\ ^3P_1$	3299.5510	30 298.404	0.098	0.055	0.563	8.47(6)	–1.16	17
	$4d^3(^2P)5s\ ^3P_2$	3303.3216	30 263.848	0.114	0.093	0.819	1.43(7)	–0.93	15
	$4d^3(^2D2)5s\ ^3D_2$	3909.3197	25 572.655	0.022	0.008	0.361	1.22(6)	–1.85	32
	$4d^3(^2P)5s\ ^1P_1$	4185.5335	23 885.074	0.048	0.042	0.890	6.46(6)	–1.07	32
	Residual				0.212				
$4d^3(^4P)5p\ ^5D^\circ_4$	$4d^4\ ^5D_3$	2263.3106	44 169.386	0.014	0.010	0.709	1.85(6)	–1.89	20
	$4d^4\ ^5D_4$	2285.2235	43 745.889	0.066	0.054	0.813	1.04(7)	–1.14	12
44970.71 cm^{-1}	$4d^3(^4P)5s\ ^5P_3$	2972.5710	33 631.122	0.890	0.907	1.020	1.75(8)	0.32	10
	$4d^3(^4F)5s\ ^3F_4$	3193.4495	31 305.026	0.008	0.006	0.857	1.24(6)	–1.77	52
	Residual				0.023				
$4d^3(^2P)5p\ ^3D^\circ_3$	$4d^4\ ^5D_4$	2242.5800	44 577.650	0.017	0.055	3.162	1.20(7)	–1.20	10
	$4d^4\ ^3F_4$	2667.1467	37 482.100	0.068	0.157	2.300	3.41(7)	–0.59	9
45802.47 cm^{-1}	$4d^4\ ^3H_4$	2754.5496	36 292.869	0.123	0.105	0.852	2.27(7)	–0.74	11
	$4d^4\ ^1D_2$	2980.7132	33 539.252	0.217	0.251	1.158	5.46(7)	–0.29	11
	$4d^4\ ^3D_2$	3029.7413	32 996.508	0.120	0.087	0.722	1.88(7)	–0.74	16
	$4d^3(^4F)5s\ ^3F_4$	3110.7976	32 136.787	0.029	0.021	0.730	4.62(6)	–1.33	28
	$4d^3(^4F)5s\ ^3F_3$	3113.1748	32 112.245	0.012	0.029	2.370	6.32(6)	–1.19	21
	$4d^3(^2G)5s\ ^3G_3$	3304.7036	30 251.221	0.161	0.067	0.415	1.46(7)	–0.78	14
	$4d^3(^2G)5s\ ^3G_4$	3348.7755	29 853.103	0.074	0.050	0.675	1.08(7)	–0.90	14
	$4d^3(^2H)5s\ ^3H_4$	3528.4778	28 332.703	0.078	0.078	1.002	1.70(7)	–0.66	17
	Residual				0.101				
$4d^3(^2H)5p\ ^3H^\circ_6$	$4d^4\ ^3H_5$	2566.0734	38 958.386	0.021	0.013	0.621	3.06(6)	–1.41	14
	$4d^4\ ^3H_6$	2590.9428	38 584.448	0.358	0.478	1.333	1.14(8)	0.17	11
48770.84 cm^{-1}	$4d^4\ ^3G_5$	2641.0561	37 852.364	0.031	0.042	1.362	1.01(7)	–0.86	12
	$4d^3(^2G)5s\ ^3G_5$	3055.5159	32 718.166	0.257	0.095	0.368	2.25(7)	–0.39	24
	$4d^3(^2H)5s\ ^3H_5$	3175.8669	31 478.359	0.246	0.252	1.024	5.99(7)	0.07	17
	$4d^3(^2H)5s\ ^3H_6$	3189.2788	31 345.949	0.086	0.120	1.393	2.86(7)	–0.25	20
	Residual				0.001				

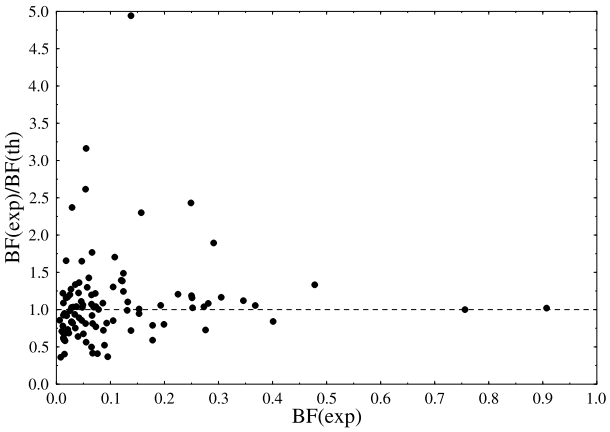

Fig. 1. The ratio of our experimental to theoretical *BF*s plotted against the experimental *BF*s.

For the convenience of the user, the Nb II wavelengths and oscillator strengths (log gf-values) are sorted by increasing wavelengths in Table 3. The wavenumbers and wavelengths are derived from energy levels reported by Ryabtsev et al. (2000). The starred wavelengths and the corresponding oscillator strengths are taken from Nilsson & Ivarsson (2008).

3. Hyperfine structure

Niobium has a nuclear spin of 9/2 and a magnetic moment $\mu/\mu_N = 6.2$ (Sheriff & Williams 1951). Therefore, many of the lines manifest hyperfine structure (hfs) effects as illustrated in Fig. 2 for the $4d^3(^4F)5s\ a^5F_5 - 4d^3(^4F)5p\ z\ ^3F^\circ_4$ transition in Nb II at 2745.31 Å. The upper levels investigated in this paper are highly excited 5p levels that interact only weakly with the nucleus and thus have a small hfs. The hfs in the lower levels is generally far more significant, especially for the 5s levels that penetrate the nucleus to a higher extent. Magnetic dipole hfs constants ($A_{\rm hfs}$) for many of the lower levels involved in the transitions reported here were published by Nilsson & Ivarsson (2008). In Table 5, we indicate the hfs of the $^5F_1 - z\ ^5G^\circ_2$, a $^5F_2 - z\ ^5G^\circ_3$, a $^5F_3 - z\ ^5G^\circ_3$, a $^5F_4 - z\ ^5G^\circ_4$, a $^3P_1 - z\ ^3D^\circ_2$, a $^3F_3 - z\ ^3D^\circ_2$, and $^3F_2 - z\ ^3G^\circ_3$ transitions, which are of astrophysical interest. The relative intensities for the components of the hypermultiplets have been calculated assuming LS coupling. This hfs information is required for calculations of stellar line profiles, which are necessary for accurate abundance determinations.

4. The theoretical model

The first analysis of Nb II was that of Humphreys & Meggers (1945). They published a list of 1494 lines in the 2002–7026 Å spectral region, which were identified as transitions between 183 Nb II levels belonging to the $4d^4$, $4d^35s$, $4d^35p$ and $4d^25s5p$ configurations. More recent measurements for the region 1579 to 2211 Å were provided by Iglesias (1954), who identified 20 new levels, mostly belonging to the $4d^25s5p$ configuration. The most recent analysis was that of Ryabtsev et al. (2000), who confirmed all but three of the previously known levels and found 153 additional Nb II levels, giving a total of 353 known levels. We used the energy levels of Ryabtsev et al. (2000).

Table 3. Experimental oscillator strengths (log gf) in Nb II sorted by air wavelengths.

$\lambda_{\rm air}$ (Å)	σ (cm^{-1})	Lower level (cm^{-1})	Log(gf)
2242.5800	44 577.650	1224.823	−1.20
2263.3106	44 169.386	801.326	−1.89
2265.6748	44 123.277	801.326	−1.37
2285.2235	43 745.889	1224.823	−1.14
2291.3844	43 628.304	438.361	−2.29
2300.2897	43 459.407	158.984	−2.12
2300.8551	43 448.717	438.361	−1.96
2315.1745	43 180.030	438.361	−1.63
2320.2400	43 085.752	801.326	−1.57
2332.8990	42 851.977	438.361	−1.93
2334.8014	42 817.065	801.326	−1.75
2343.2745	42 662.255	1224.823	−1.92
2372.7316	42 132.646	0.000	−2.31
2381.7200	41 973.662	158.984	−2.22
2514.3531	39 759.692	801.326	−1.76
2541.4244	39 336.195	1224.823	−1.02
2566.0734	38 958.386	9812.452	−1.41
2590.9428	38 584.448	10186.390	+0.17
2641.0561	37 852.364	10918.474	−0.86
2646.253⋆	37 778.026	438.361	−0.55
2656.075⋆	37 638.332	158.984	−0.61
2666.590⋆	37 489.926	801.326	−0.79
2667.1467	37 482.100	8320.373	−0.59
2667.291⋆	37 480.076	0.000	−0.77
2671.6567	37 418.838	7505.765	−1.30
2671.926⋆	37 415.061	801.326	−0.33
2675.939⋆	37 358.955	438.361	−0.73
2678.654⋆	37 321.092	158.984	−1.56
2691.770⋆	37 139.258	158.984	−0.79
2697.059⋆	37 066.429	1224.823	+0.06
2698.858⋆	37 041.715	438.361	−0.56
2700.1527	37 023.959	7900.644	−0.68
2700.5523	37 018.457	3542.561	−1.27
2702.194⋆	36 995.990	801.326	−0.51
2702.517⋆	36 991.564	1224.823	−0.75
2706.397⋆	36 938.540	438.361	−1.25
2716.306⋆	36 803.790	158.984	−1.18
2716.622⋆	36 799.513	1224.823	−0.24
2721.630⋆	36 731.805	0.000	−1.42
2721.982⋆	36 727.056	801.326	−0.29
2729.5123	36 625.754	7261.324	−1.77
2733.256⋆	36 575.575	801.326	−0.60
2733.462⋆	36 572.821	158.984	−1.05
2734.3521	36 560.900	7505.765	−1.19
2737.085⋆	36 524.413	438.361	−0.87
2745.3118	36 414.981	4146.037	−0.86
2747.3562	36 387.869	7261.324	−0.94
2749.6848	36 357.067	7261.324	−1.32
2754.5496	36 292.869	9509.604	−0.74
2765.9299	36 143.428	7505.765	−1.45
2768.124⋆	36 114.877	438.361	−0.50
2780.235⋆	35 957.568	4146.037	−0.40
2793.041⋆	35 792.709	3542.561	−0.71
2793.6766	35 784.573	7505.765	−1.43
2798.9044	35 717.747	7900.644	−1.03
2810.7918	35 566.705	8320.373	−0.69
2827.075⋆	35 361.838	158.984	−0.83
2829.750⋆	35 328.415	1224.823	−1.55
2841.143⋆	35 186.758	3029.629	−0.69
2842.643⋆	35 168.184	2629.132	−0.59
2846.279⋆	35 123.260	2356.816	−0.73
2861.092⋆	34 941.426	2356.816	−0.68
2865.609⋆	34 886.354	0.000	−1.18
2866.8425	34 871.322	7261.324	−2.13

Table 3. continued.

λ_{air} (Å)	σ (cm^{-1})	Lower level (cm^{-1})	Log(gf)
2887.0836	34 626.881	7505.765	−1.52
2917.0516	34 271.176	10653.427	−0.66
2956.8884	33 809.499	7900.644	−1.29
2868.521⋆	34 850.944	2629.132	−0.37
2875.390⋆	34 767.687	3029.629	−0.17
2877.038⋆	34 747.769	2629.132	−0.39
2883.174⋆	34 673.826	3542.561	−0.04
2888.829⋆	34 605.958	2356.816	−0.59
2897.806⋆	34 498.753	3029.629	−0.37
2899.233⋆	34 481.775	3542.561	−0.34
2908.240⋆	34 374.989	2356.816	−0.40
2910.587⋆	34 347.272	3029.629	−0.16
2911.742⋆	34 333.642	2629.132	−0.28
2927.811⋆	34 145.215	4146.037	+0.16
2931.464⋆	34 102.673	2629.132	−0.92
2941.543⋆	33 985.821	3542.561	−0.05
2946.895⋆	33 924.106	2629.132	−1.00
2950.880⋆	33 878.299	4146.037	+0.24
2972.5710	33 631.122	11339.590	+0.32
2980.7132	33 539.252	12263.221	−0.29
2982.102⋆	33 523.609	3029.629	−0.85
2991.9493	33 413.238	10653.427	−0.76
2994.722⋆	33 382.345	4146.037	−0.29
3014.439⋆	33 164.006	2356.816	−1.61
3024.7316	33 051.241	10835.837	−0.18
3028.441⋆	33 010.677	3542.561	−0.20
3029.7413	32 996.508	12805.965	−0.74
3029.8088	32 995.766	10653.427	−1.11
3032.6351	32 964.964	10653.427	−1.26
3039.397⋆	32 891.690	2629.132	−1.26
3049.5039	32 782.554	10835.837	−1.04
3055.5159	32 718.166	16052.672	−0.39
3063.1193	32 636.911	10653.427	−0.91
3071.5463	32 547.488	11339.590	−0.29
3073.236⋆	32 529.538	2356.816	−1.19
3074.270⋆	32 518.595	7261.324	−1.69
3076.863⋆	32 491.193	3029.629	−0.55
3080.3475	32 454.501	10835.837	−0.48
3094.174⋆	32 309.420	4146.037	+0.56
3097.1160	32 278.801	11339.590	−0.84
3099.181⋆	32 257.222	2629.132	−0.93
3100.7738	32 240.645	8320.373	−1.30
3110.7976	32 136.787	13665.686	−1.33
3113.1748	32 112.245	13690.228	−1.19
3128.9145	31 950.748	11339.590	−1.34
3129.6522	31 943.127	10653.427	−0.81
3130.783⋆	31 931.636	3542.561	+0.41
3135.925⋆	31 879.275	7900.644	−1.32
3145.402⋆	31 783.232	8320.373	+0.12
3163.140⋆	31 605.006	6192.310	−1.38
3163.401⋆	31 602.404	3029.629	+0.27
3175.7747	31 479.219	10653.427	−0.78
3175.8669	31 478.359	17292.479	+0.07
3177.766⋆	31 459.546	8320.374	−1.80
3179.2265	31 445.143	13479.460	−1.53
3180.285⋆	31 434.626	7900.644	+0.10
3181.398⋆	31 423.636	7261.324	−1.12
3188.3466	31 355.170	12263.221	−1.59
3189.2788	31 345.949	17424.889	−0.25
3191.094⋆	31 328.160	4146.037	−0.33
3193.4495	31 305.026	13665.686	−1.77
3194.2782	31 296.809	10835.837	−0.77
3194.974⋆	31 290.112	2629.132	+0.12
3206.340⋆	31 179.195	7505.765	+0.04

Table 3. continued.

λ_{air} (Å)	σ (cm^{-1})	Lower level (cm^{-1})	Log(gf)
3207.331⋆	31 169.564	5562.241	−1.37
3215.594⋆	31 089.472	8320.374	−0.24
3216.187⋆	31 083.743	7900.644	−1.52
3222.0580	31 027.117	12263.221	−0.73
3223.326⋆	31 014.897	8320.374	−0.74
3225.471⋆	30 994.274	2356.816	−0.01
3229.557⋆	30 955.063	7261.324	−0.75
3236.400⋆	30 889.615	7900.644	−0.30
3237.9954	30 874.306	10835.837	−0.72
3242.4077	30 832.382	13054.696	−1.47
3244.5078	30 812.426	12805.965	−1.26
3247.470⋆	30 784.316	7900.644	−0.74
3248.932⋆	30 770.464	6192.310	−1.11
3254.062⋆	30 721.958	2629.132	−0.50
3267.673⋆	30 594.001	10604.229	−1.38
3273.505⋆	30 539.495	6192.310	−1.55
3273.880⋆	30 535.992	7261.324	−1.68
3277.7583	30 499.863	13118.528	−1.66
3291.051⋆	30 376.683	3542.561	−1.54
3297.045⋆	30 321.461	3029.629	−1.63
3299.5510	30 298.404	14626.199	−1.16
3302.616⋆	30 270.315	9509.604	−1.49
3303.3216	30 263.848	14660.755	−0.93
3304.7036	30 251.221	15551.252	−0.78
3319.585⋆	30 115.577	7261.324	−0.91
3340.3740	29 928.163	13690.228	−1.59
3341.596⋆	29 917.215	10186.390	−0.46
3343.892⋆	29 896.672	7900.644	−1.31
3343.966⋆	29 896.014	8320.374	−0.89
3346.751⋆	29 871.136	7505.765	−1.23
3348.7755	29 853.103	15949.370	−0.90
3365.587⋆	29 703.963	8320.374	−0.74
3365.872⋆	29 701.450	7261.324	−1.54
3372.5601	29 642.544	10918.474	−0.80
3374.246⋆	29 627.738	7900.644	−1.19
3386.238⋆	29 522.818	9812.452	−0.46
3388.929⋆	29 499.376	10604.229	−1.31
3391.587⋆	29 476.257	7900.644	−1.85
3394.9714	29 446.922	12263.221	−0.80
3395.7224	29 440.466	14626.199	−1.28
3399.7112	29 405.910	14660.755	−0.63
3408.673⋆	29 328.512	6192.310	−0.58
3409.185⋆	29 324.113	5562.241	−0.87
3412.932⋆	29 291.914	7261.324	−0.50
3420.625⋆	29 226.040	7505.765	−1.12
3421.1646	29 221.428	11339.590	−1.36
3425.420⋆	29 185.131	10918.474	−0.26
3426.528⋆	29 175.690	10604.229	−0.78
3426.568⋆	29 175.356	9509.604	−0.50
3436.821⋆	29 088.315	10246.955	−1.30
3439.918⋆	29 062.130	7900.644	−1.04
3440.581⋆	29 056.528	8320.373	−0.69
3448.2179	28 992.192	14626.199	−1.06
3448.6696	28 988.438	14660.755	−1.09
3450.7619	28 970.875	14678.318	−0.90
3452.3409	28 957.636	14660.755	−0.70
3478.786⋆	28 737.432	10246.955	−0.84
3479.560⋆	28 731.041	10604.229	−0.46
3484.046⋆	28 694.044	6192.310	−1.06
3489.087⋆	28 652.594	7900.644	−1.08
3515.416⋆	28 438.005	10246.955	−0.59
3528.4778	28 332.703	17469.770	−0.66
3537.622⋆	28 259.498	7261.324	−0.96

Table 3. continued.

λ_{air} (Å)	σ (cm^{-1})	Lower level (cm^{-1})	Log(gf)
3540.959⋆	28 232.865	8320.373	−0.43
3541.2454	28 230.683	13479.460	−0.85
3591.194⋆	27 837.946	10186.390	−1.31
3619.509⋆	27 620.178	7900.644	−0.42
3633.121⋆	27 516.698	12263.221	−1.53
3639.0501	27 471.891	14660.755	−0.98
3641.3782	27 454.328	14678.318	−1.56
3651.182⋆	27 380.589	7505.765	−0.48
3688.189⋆	27 105.862	10918.474	−1.44
3691.1738	27 083.944	14626.199	−1.24
3695.8960	27 049.388	14660.755	−0.62
3717.0600	26 895.332	13665.686	+0.03
3720.4532	26 870.790	13690.228	−0.51
3740.720⋆	26 725.223	13054.696	−0.31
3741.288⋆	26 721.166	12263.221	−1.39
3781.372⋆	26 437.919	13665.686	−0.47
3801.136⋆	26 300.459	13479.460	−0.65
3804.012⋆	26 280.574	13054.696	−0.98
3818.856⋆	26 178.422	12805.965	−0.22
3828.243⋆	26 114.233	13665.686	−0.86
3831.844⋆	26 089.691	13690.228	−0.25
3855.489⋆	25 929.691	13054.696	−1.17
3863.042⋆	25 878.995	12805.965	−0.85
3865.004⋆	25 865.859	13118.528	−0.83
3879.3421	25 770.263	14790.755	−0.55
3898.285⋆	25 645.042	13690.228	−0.69
3909.3197	25 572.655	19351.948	−1.85
3919.701⋆	25 504.927	13479.460	−0.93
3949.445⋆	25 312.850	14790.755	−1.06
3952.363⋆	25 294.159	13690.228	−0.93
4000.603⋆	24 989.164	14790.755	−1.03
4026.3014	24 829.673	18819.520	−1.53
4059.674⋆	24 625.566	13665.686	−1.18
4061.9711	24 611.648	15949.370	−1.02
4073.080⋆	24 544.515	14790.755	−1.36
4085.3468	24 470.818	18819.520	−1.28
4104.160⋆	24 358.650	13665.686	−1.24
4110.309⋆	24 322.205	13054.696	−1.61
4114.5320	24 297.245	19351.948	−1.44
4126.178⋆	24 228.667	15551.252	−1.49
4138.452⋆	24 156.809	12805.965	−1.65
4156.671⋆	24 050.933	16052.672	−1.12
4185.5335	23 885.074	21039.529	−1.07
4216.226⋆	23 711.215	13665.686	−1.45
4254.385⋆	23 498.542	13054.696	−1.23
4321.481⋆	23 133.708	15551.252	−1.20
4367.3789	22 890.623	18819.520	−1.19
4367.960⋆	22 887.552	13665.686	−1.03
4421.6458	22 609.664	21039.529	−1.31
4467.8849	22 375.702	21511.376	−1.26
4492.9563	22 250.809	21039.529	−0.87
4522.1931	22 107.015	21511.376	−1.20
4527.636⋆	22 080.389	12805.965	−1.29
4579.444⋆	21 830.594	13690.228	−1.02
4588.9970	21 785.149	20347.497	−1.46
4699.5812	21 272.640	20437.503	−1.04

Notes. For the starred values, see the text.

Our knowledge of the Nb III spectrum remains incomplete. Only 19 levels were reported by Moore (1958), which were deduced from the pioneering work of Gibbs & White (1928) and Eliason (1933). Additional work performed by Iglesias (1955) established 58 new levels belonging to the 4d^3, 4d^{2}5s, 4d^{2}5d, 4d^{2}6s, and 4d^{2}5p configurations. The most recent analysis of this

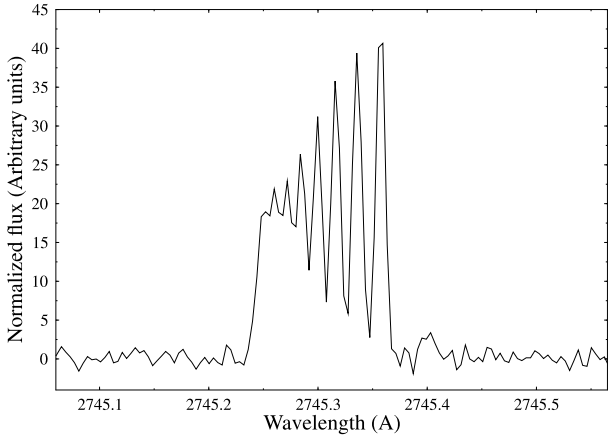

Fig. 2. The 4d^3(^{4}F)5s a^{5}F$_5$–4d^3(^{4}F)5p z ^{3}F$^\circ_4$ transition in Nb II at 2745.31 Å. The large structure (more than 0.1 Å) is produced by the hfs splitting in the 4d^3(^{4}F)5s a ^{5}F$_5$ energy level (Nilsson & Ivarsson 2008).

spectrum was completed by Gayazov et al. (1998), who identified 908 transitions.

Atomic structure calculations in Nb II–Nb III are realistic only if relativistic and correlation effects are considered simultaneously. As has been frequently discussed (e.g., Biémont & Quinet 2003; Biémont 2005), the HFR approach developed by Cowan (1981), although based on the non-relativistic Schrödinger equation, is well suited to heavy atoms or ions because it incorporates the most significant relativistic effects (Blume-Watson spin-orbit interaction, mass-velocity, and one-body Darwin terms). This HFR approach was adopted here. Configuration interaction (CI) was included in the calculations extensively. In addition, a least squares fitting procedure was applied to the radial integrals using the experimental energy levels.

In Nb II, two different physical models were considered. In the first model (designated HFR(A)), a 4d ionic core surrounded by 3 valence electrons was chosen. Valence-valence type interactions were considered by including the following configurations in the CI expansions: 4d^4, 4d^{3}5s, 4d^{3}6s, 4d^{3}5d, 4d^{2}5s^2, 4d^{2}5p^2, 4d^{2}5s6s, 4d^{2}5s5d, 4d5s^{2}6s, and 4d5s5p^2 (even parity), and 4d^{3}5p, 4d^{3}4f, 4d^{3}5f, 4d^{2}5s5p, 4d^{2}4f5s, 4d^{2}5s5f, 4d^{2}5p6s, 4d^{2}5p5d, 4d^{2}4f5d, and 4d5s^{2}5p (odd parity).

Core-valence interactions were taken into account using a polarization model potential and a correction to the dipole operator following a well-established procedure (see Biémont & Quinet 2003; Quinet et al. 1999) giving rise to the HFR+CPOL method.

In the present context, the polarization model for Nb II was based on a Nb^{4+} ionic core surrounded by 3 valence electrons. For the dipole polarizability α_d, we used the value calculated by Fraga et al. (1976), i.e., $\alpha_d = 3.64\ a_0^3$, corresponding to the ionic core Nb V. The value of the cut-off radius r_c was the HFR mean value $\langle r \rangle$ of the outermost 4d core orbital, i.e., $r_c = 1.85\ a_0$.

The HFR+CPOL method was combined with a least squares optimization routine that minimized the discrepancies between calculated and experimental energy levels published by Ryabtsev et al. (2000). In the fitting process, we included all the experimentally known energy levels below 80 000 cm^{-1}. These levels belong to the 4d^4, 4d^{3}5s, 4d^{3}6s, 4d^{3}5d, and 4d^{2}5s^2 configurations (even parity) and to the 4d^{3}5p and 4d^{2}5s5p configurations (odd parity). For these configurations, the fitted parameters were the center-of-gravity energies (E_{av}), both the single-configuration direct (F^k) and exchange (G^k) electrostatic

Table 4. Comparison between theoretical f-values obtained in this work for Nb II and those calculated previously.

Lower level[a]		Upper level[a]		f-value	f-values RCI[b]	
Desig.	E(cm^{-1})	Desig.	E(cm^{-1})	this work	velocity	length
$4d^3(^4F)5s\ ^5F_2$	2629.13	$4d^3(^4F)5p\ ^5G^\circ_3$	33 919.24	0.277	0.239	0.315
$4d^3(^4F)5s\ ^5F_3$	3029.63	$4d^3(^4F)5p\ ^5G^\circ_3$	33 919.24	0.072	0.065	0.074
$4d^4\ ^5D_2$	438.36	$4d^3(^4F)5p\ ^3D^\circ_3$	36 553.24	0.064	0.054	0.068
$4d^3(^4F)5s\ ^5F_2$	2629.13	$4d^3(^4F)5p\ ^3D^\circ_3$	36 553.24	0.022	0.020	0.027
$4d^3(^4F)5s\ ^5F_3$	3029.63	$4d^3(^4F)5p\ ^3D^\circ_3$	36 553.24	0.022	0.026	0.031
$4d^3(^4F)5s\ ^5F_4$	3542.56	$4d^3(^4F)5p\ ^3D^\circ_3$	36 553.24	0.065	0.052	0.068
$4d^4\ ^3P_2$	7261.32	$4d^3(^4F)5p\ ^3D^\circ_3$	36 553.24	0.051	0.065	0.069
$4d^4\ ^3F_4$	8320.37	$4d^3(^4F)5p\ ^3D^\circ_3$	36 553.24	0.040	0.038	0.041

Notes. [(a)] Ryabtsev et al. (2000); [(b)] Beck & Datta (1995).

interaction integrals and the spin-orbit parameters (ζ_{nl}). All the non-fitted F^k, G^k, and R^k integrals were scaled by a factor of 0.85 as suggested by Cowan (1981), while the ab initio values of the spin-orbit parameters were used. The standard deviations of the fits were found to be equal to 296 cm^{-1} and 292 cm^{-1} for the even and odd parities, respectively.

In the second model (referred to as HFR(B)), a $4d^2$ ionic core surrounded by 2 valence electrons was considered. The valence-valence interactions were taken into account by including the following configurations on a vectorial basis: $4d^4$, $4d^35s$, $4d^36s$, $4d^35d$, $4d^25s^2$, $4d^25p^2$, $4d^25s6s$, $4d^25s5d$, $4d^24f5p$, $4d^25p5f$, $4d^26s^2$, $4d^25d^2$, $4d^25d6s$, and $4d^25p6p$ (even parity), and $4d^35p$, $4d^36p$, $4d^34f$, $4d^35f$, $4d^25s5p$, $4d^25s6p$, $4d^24f5s$, $4d^24f5d$, $4d^25s5f$, $4d^25p6s$, $4d^25p5d$, and $4d^26s6p$ (odd parity). In this model, the CPOL effects were included using the dipole polarizability corresponding to the ionic Nb IV core given in Fraga et al. (1976), i.e., $\alpha_d = 5.80\ a_0^3$. As previously, the cut-off radius was chosen to be equal to $r_c = 1.85\ a_0$.

For the odd parity, the fitting procedure was more complicated, partly because of the poor knowledge of the $4d5s^25p$ configuration. Since all the experimental lifetimes obtained for Nb II correspond to $4d^35p$ levels, we focused on the low-lying $4d^35p$ configuration including the odd experimental levels below 50 000 cm^{-1}. The parameters of the $4d^25s5p$ configuration were not adjusted, except for the center-of-gravity energy (E_{av}). The standard deviations of the fits were found to be 280 cm^{-1} and 148 cm^{-1} for the even and odd parities, respectively[1].

Table 1 shows a comparison between lifetimes calculated with the two theoretical models HFR(A) and HFR(B). We can see that the HFR(A) results appear systematically shorter than the experimental values (on average by 12%). This is probably caused by our not introducing a sufficient number of $4d^2nln'l'$ configurations to accurately account for the valence-valence interactions. Because of computer limitations, it was impossible to add more configurations of this type to the HFR(A) model. Consequently, we considered a second model with additional $4d^2nln'l'$ configurations and a $4d^2$ ionic core surrounded by 2 valence electrons (HFR(B) model). From Table 1, we can see that there is good agreement between the HFR(B) results and the experimental lifetimes (within 4%). However, for the $4d^3(^4F)5p\ ^5D^\circ$ levels, the values obtained by Hannaford et al. (1985) are about 10% longer than the lifetimes measured in the present work. The excellent agreement of the HFR+CPOL lifetimes with the new measurements presented here indicate that the measurements of lifetimes by Hannaford et al. (1985) could be too long.

Table 4 compares the HFR oscillator strengths with those previously published by Beck & Datta (1995) and shows that the agreement is very good.

Using the HFR(B) model, a particularly close agreement is found between theory and experiment for the lifetimes (see Table 1). Consequently, we decided to adopt a similar model for Nb III, an ion for which no experimental lifetimes at all are available. In this case, the following configurations were included: $4d^3$, $4d^25s$, $4d^26s$, $4d^25d$, $4d5s^2$, $4d5p^2$, $4d5s6s$, $4d5s5d$, $4d5p4f$, $4d5p5f$, $4d6s^2$, $4d5d^2$, $4d5d6s$, $4d5p6p$ (even parity), and $4d^25p$, $4d^26p$, $4d^24f$, $4d^25f$, $4d5s5p$, $4d5s6p$, $4d4f5s$, $4d4f5d$, $4d5s5f$, $4d5p6s$, $4d5p5d$, and $4d6s6p$ (odd parity).

As far as polarization effects are concerned, a Nb^{4+} ionic core was considered to be surrounded by a valence electron. For the dipole polarizability α_d, we used the value calculated by Fraga et al. (1976), i.e., $\alpha_d = 3.64\ a_0^3$. The value of the cut-off radius r_c was the HFR mean value $\langle r \rangle$ of the outermost 4d core orbital, i.e., $r_c = 1.85\ a_0$.

In the fitting procedure, we used the experimentally established levels from Iglesias (1955). For the even parity, all the available experimental levels were included in the fitting procedure. For the odd parity, several levels were not established with certainty and were marked with a question mark (?) in Iglesias' analysis or were not adequately reproduced in our calculations. Consequently, we excluded the levels at 85 999.3, 74 907.7, 85 585.1, 83 259.4, and 81 953.4 cm^{-1} from the fitting procedure.

The standard deviations of the fitting procedures were 197 cm^{-1} (even levels) and 248 cm^{-1} (odd levels). The lifetime values obtained in Nb III (with and without polarization effects) are reported in Table 6, only the values larger than 1 ns being quoted to limit the length of the table.

The oscillator strengths (log gf-values) and transition probabilities (gA) of the most intense transitions in Nb III are reported in Table 7. We verified that none of these transitions were affected by cancellation effects in the line strengths (Cowan 1981).

5. Solar and stellar abundances

Using the new Nb II transition data, we rederived niobium abundances in the solar photosphere and in five n-capture-rich metal-poor giant stars. In general, we followed procedures that have been used in a number of papers on the rare-earth elements (Sneden et al. 2009, and references therein).

[1] Because of space limitations the values of the fitted parameters are not given here but are available upon request from the authors.

Table 5. Hyperfine splitting and oscillator strengths (log gf) for Nb II transitions.

Transition[a]	F upper	F lower	σ^b (cm^{-1})	$\lambda_{air}{}^b$ (Å)	log(gf)[b]
a ^{5}F$_1$–z ^{5}G$^\circ_2$	2.5	3.5	30 993.613	3225.540	–0.93
	3.5	3.5	30 993.756	3225.525	–1.02
	3.5	4.5	30 993.928	3225.507	–1.21
	4.5	3.5	30 993.941	3225.506	–1.32
	4.5	4.5	30 994.113	3225.488	–0.90
	4.5	5.5	30 994.323	3225.466	–1.67
	5.5	4.5	30 994.338	3225.464	–0.86
	5.5	5.5	30 994.548	3225.443	–1.02
	6.5	5.5	30 994.815	3225.415	–0.56
a ^{5}F$_2$–z ^{5}G$^\circ_3$	1.5	2.5	31 289.962	3194.990	–1.12
	2.5	2.5	31 290.014	3194.984	–1.23
	2.5	3.5	31 289.954	3194.990	–1.27
	3.5	2.5	31 290.085	3194.977	–1.63
	3.5	3.5	31 290.025	3194.983	–1.04
	3.5	4.5	31 289.948	3194.991	–1.45
	4.5	3.5	31 290.118	3194.974	–1.19
	4.5	4.5	31 290.040	3194.982	–0.98
	4.5	5.5	31 289.946	3194.991	–1.72
	5.5	4.5	31 290.153	3194.970	–0.90
	5.5	5.5	31 290.059	3194.980	–1.03
	5.5	6.5	31 289.948	3194.991	–2.16
	6.5	5.5	31 290.192	3194.966	–0.69
	6.5	6.5	31 290.081	3194.977	–1.22
	7.5	6.5	31 290.235	3194.962	–0.52
a ^{5}F$_3$–z ^{5}G$^\circ_3$	1.5	1.5	30 889.762	3236.385	–1.89
	1.5	2.5	30 889.689	3236.392	–1.80
	2.5	1.5	30 889.813	3236.379	–1.80
	2.5	2.5	30 889.740	3236.387	–2.79
	2.5	3.5	30 889.637	3236.398	–1.59
	3.5	2.5	30 889.812	3236.379	–1.59
	3.5	3.5	30 889.709	3236.390	–3.17
	3.5	4.5	30 889.576	3236.404	–1.51
	4.5	3.5	30 889.801	3236.380	–1.51
	4.5	4.5	30 889.669	3236.394	–2.06
	4.5	5.5	30 889.507	3236.411	–1.50
	5.5	4.5	30 889.781	3236.383	–1.50
	5.5	5.5	30 889.620	3236.399	–1.58
	5.5	6.5	30 889.428	3236.420	–1.56
	6.5	5.5	30 889.753	3236.386	–1.56
	6.5	6.5	30 889.562	3236.406	–1.25
	6.5	7.5	30 889.341	3236.429	–1.76
	7.5	6.5	30 889.715	3236.389	–1.76
	7.5	7.5	30 889.495	3236.413	–1.01
a ^{5}F$_4$–z ^{5}G$^\circ_4$	0.5	0.5	31 089.935	3215.546	–2.46
	0.5	1.5	31 089.886	3215.551	–2.02
	1.5	0.5	31 089.953	3215.544	–2.02
	1.5	1.5	31 089.904	3215.550	–4.06
	1.5	2.5	31 089.821	3215.558	–1.79
	2.5	1.5	31 089.934	3215.546	–1.79
	2.5	2.5	31 089.851	3215.555	–3.05
	2.5	3.5	31 089.736	3215.567	–1.67
	3.5	2.5	31 089.893	3215.551	–1.67
	3.5	3.5	31 089.777	3215.563	–2.30
	3.5	4.5	31 089.629	3215.578	–1.60
	4.5	3.5	31 089.831	3215.557	–1.60
	4.5	4.5	31 089.683	3215.572	–1.88
	4.5	5.5	31 089.501	3215.591	–1.58
	5.5	4.5	31 089.748	3215.566	–1.58
	5.5	5.5	31 089.567	3215.584	–1.58
	5.5	6.5	31 089.352	3215.607	–1.60
	6.5	5.5	31 089.645	3215.576	–1.60
	6.5	6.5	31 089.430	3215.599	–1.35
	6.5	7.5	31 089.182	3215.624	–1.69
	7.5	6.5	31 089.520	3215.589	–1.69
	7.5	7.5	31 089.272	3215.615	–1.15
	7.5	8.5	31 088.991	3215.644	–1.91
	8.5	7.5	31 089.374	3215.604	–1.91
	8.5	8.5	31 089.093	3215.633	–0.98
a ^{3}P$_1$–z ^{3}D$^\circ_2$	2.5	3.5	29 328.450	3408.681	–1.50
	3.5	3.5	29 328.474	3408.678	–1.59
	3.5	4.5	29 328.463	3408.679	–1.79
	4.5	3.5	29 328.504	3408.674	–1.89
	4.5	4.5	29 328.494	3408.676	–1.47
	4.5	5.5	29 328.481	3408.677	–2.24
	5.5	4.5	29 328.531	3408.671	–1.43
	5.5	5.5	29 328.519	3408.673	–1.59
	6.5	5.5	29 328.563	3408.668	–1.13
a ^{3}F$_3$–z ^{3}D$^\circ_2$	2.5	1.5	27 620.210	3619.505	–1.66
	2.5	2.5	27 620.194	3619.507	–1.76
	2.5	3.5	27 620.171	3619.510	–2.16
	3.5	2.5	27 620.218	3619.504	–1.81
	3.5	3.5	27 620.195	3619.507	–1.57
	3.5	4.5	27 620.166	3619.511	–1.72
	4.5	3.5	27 620.226	3619.503	–1.99
	4.5	4.5	27 620.197	3619.507	–1.52
	4.5	5.5	27 620.161	3619.512	–1.44
	5.5	4.5	27 620.234	3619.502	–2.25
	5.5	5.5	27 620.198	3619.507	–1.56
	5.5	6.5	27 620.156	3619.512	–1.23
	6.5	5.5	27 620.242	3619.501	–2.69
	6.5	6.5	27 620.200	3619.506	–1.75
	6.5	7.5	27 620.151	3619.513	–1.06
a ^{3}F$_2$–z ^{3}G$^\circ_3$	1.5	2.5	31 179.159	3206.344	–1.21
	2.5	2.5	31 179.216	3206.338	–1.31
	2.5	3.5	31 179.109	3206.349	–1.35
	3.5	2.5	31 179.294	3206.330	–1.71
	3.5	3.5	31 179.188	3206.341	–1.12
	3.5	4.5	31 179.050	3206.355	–1.54
	4.5	3.5	31 179.289	3206.331	–1.27
	4.5	4.5	31 179.152	3206.345	–1.07
	4.5	5.5	31 178.984	3206.362	–1.80
	5.5	4.5	31 179.275	3206.332	–0.99
	5.5	5.5	31 179.108	3206.349	–1.11
	5.5	6.5	31 178.909	3206.370	–2.24
	6.5	5.5	31 179.254	3206.334	–0.77
	6.5	6.5	31 179.056	3206.355	–1.30
	7.5	6.5	31 179.224	3206.337	–0.60

Notes. [(a)] Level designations and center of gravity energies from Ryabtsev et al. (2000); [(b)] derived from the data reported by Nilsson & Ivarsson (2008).

5.1. Line selection

The principal difficulty for Nb II abundance studies is that there are no strong transitions in the visible spectral range. It is thus necessary to utilize the crowded UV region, where few if any transitions are unblended, and placement of the stellar continuum is often very uncertain. In Fig. 3, we plot the relative strengths of Nb II lines as a function of wavelength. Details of the line strength arguments can be found in Sneden et al. (2009) and references therein. Briefly, to first approximation the relative logarithmic absorption strength of a transition within a particular species is proportional to log $gf - \theta\chi$, where χ is the excitation potential in eV and θ = 5040/T, the inverse temperature. Additionally, the first ionization potential for niobium is

Table 6. HFR lifetimes (τ in ns) (without and with core-polarization effects included) of the low-lying levels of Nb III ($4d^2 5p$ configuration). Only lifetime values larger than 1 ns are quoted.

E (cm^{-1})[a]	Term[a]	J	τ (HFR)	τ (HFR+CPOL)
63 686.7	^{4}G°	5/2	2.25	2.58
65 005.9	^{4}G°	7/2	2.13	2.44
65 904.2	^{4}F°	3/2	1.01	1.16
66 456.2	^{4}G°	9/2	2.02	2.32
66 598.4	^{2}F°	5/2	1.21	1.39
67 094.1	^{4}F°	5/2	1.20	1.37
67 775.0	^{2}D°	3/2	1.17	1.33
68 061.7	^{4}G°	11/2	1.96	2.25
68 382.1	^{2}F°	7/2	1.56	1.78
69 110.4	^{2}D°	5/2	1.20	1.37
74 726.7	^{4}D°	1/2	1.40	1.62
75 383.1	^{4}D°	3/2	1.02	1.13
76 387.8?	^{2}D°	5/2	1.00	1.16
76 913.3?	^{2}D°	3/2	1.03	1.20
77 247.5	^{2}F°	5/2	1.28	1.46
78 085.9	^{4}P°	1/2	1.16	1.34
78 372.2	^{4}P°	3/2	1.20	1.38
79 429.7	^{4}P°	5/2	1.18	1.35
82 152.1	^{2}H°	11/2	1.33	1.52
84 523.0	^{2}F°	7/2	1.08	1.23

Notes. [a] From Iglesias (1955).

relatively low (6.6 eV). In the solar and stellar photospheres considered in this paper, virtually all niobium is in the form of Nb^+; there are essentially no "Saha" corrections for other niobium ionization stages. Therefore, the relative strengths of Nb II lines can be compared to those of other ionized-species with similarly low ionization potentials (such as all of the rare-earth elements) by writing the relative strengths as $\log \epsilon gf - \theta\chi$, where ϵ is the elemental abundance. In Fig. 3, we show the adopted $\theta = 1.0$, a compromise between the $\theta_{\rm eff}$ values of the Sun and the metal-poor giant program stars. The strengths of the Nb II lines are quite sensitive to the exact choice of θ. For this figure, we also assumed that $\log \epsilon_\odot = 1.4$, which is close to the photospheric and meteoritic abundances.

In Fig. 3, we indicate the minimum strength at which Nb II lines can be detected in the solar spectrum, and the value of this quantity at which the lines become strong (so that line saturation might become an issue; see Sneden et al. 2009, and references therein). These two levels are very approximate, but for example lines with strengths < -0.6 are simply too weak to be reliably identified and used in an abundance study. They may be safely ignored in our search for useful Nb II lines. This limit (very roughly) holds also for the kinds of very metal-poor, *r*-process-rich giant stars considered in this paper.

It is clear from Fig. 3 that no detectable lines of Nb II occur above 4000 Å. This is confirmed by the Moore et al. (1966) solar line compendium. They identified 26 transitions as at least partly attributable to Nb II. Their two longest-wavelength identifications are 3818.99 and 4492.96 Å. But the latter transition (not considered in the present work or by Nilsson & Ivarsson 2008) is blended with a Ce II line (Palmeri et al. 2000; Lawler et al. 2009) that accounts for a large fraction of the very weak solar absorption at this wavelength. Its attribution to Nb II is therefore doubtful, and thus all useful Nb II transitions are in the

Table 7. Transition probabilities (gA, in s^{-1}) and oscillator strengths ($\log gf$) for the most intense transitions ($\log gf > -0.50$) of Nb III.

λ (Å)[a]	Int.[a]	Transition[a]	$\log gf$[b]	gA[b]
1431.92	60	a $^4P_{5/2}$–z $^4P°_{5/2}$	–0.46	1.13(9)
1445.43	80	a $^4F_{3/2}$–z $^4D°_{1/2}$	–0.37	1.36(9)
1445.98	80	a $^4F_{5/2}$–z $^4D°_{3/2}$	–0.20	2.02(9)
1447.09	80	a $^4F_{7/2}$–z $^4D°_{5/2}$	–0.08	2.65(9)
1448.50	50B	a $^2G_{9/2}$–y $^2G°_{9/2}$	–0.35	1.41(9)
1451.63	60	a $^2H_{11/2}$–z $^2H°_{11/2}$	0.03	3.40(9)
1456.68	100	a $^4F_{9/2}$–z $^4D°_{7/2}$	0.13	4.26(9)
1495.94	100	a $^4F_{9/2}$–z $^4F°_{9/2}$	0.26	5.44(9)
1499.45	80	a $^4F_{7/2}$–z $^4F°_{7/2}$	0.13	3.97(9)
1501.99	100	a $^4F_{5/2}$–z $^4F°_{5/2}$	–0.35	1.31(9)
1513.81	80	a $^2H_{9/2}$–y $^2G°_{7/2}$	0.39	7.08(9)
1517.38	50	a $^4F_{3/2}$–z $^4F°_{3/2}$	–0.23	1.70(9)
1524.91	100	a $^2H_{11/2}$–y $^2G°_{9/2}$	0.44	7.84(9)
1537.50	60	a $^4P_{3/2}$–z $^2P°_{3/2}$	–0.48	9.36(8)
1546.50	40	a $^2F_{7/2}$–x $^2F°_{7/2}$	–0.10	2.23(9)
1566.92	50B	a $^2D_{5/2}$–y $^2D°_{3/2}$	–0.35	1.21(9)
1590.21	100	a $^2G_{9/2}$–z $^2G°_{9/2}$	0.09	3.24(9)
1598.86	80	a $^2F_{7/2}$–x $^2D°_{5/2}$	0.08	3.14(9)
1604.72	80	a $^2G_{7/2}$–z $^2G°_{7/2}$	0.00	2.60(9)
1639.51	80	a $^4P_{5/2}$–z $^4D°_{7/2}$	–0.30	1.24(9)
1682.77	100	a $^2H_{11/2}$–z $^2G°_{9/2}$	–0.07	2.03(9)
1705.44	100	a $^2H_{9/2}$–z $^2G°_{7/2}$	–0.27	1.23(9)
1808.70	50	a $^2D_{5/2}$–z $^2F°_{7/2}$	–0.48	6.77(8)
1892.92	100	a $^2F_{7/2}$–z $^2G°_{9/2}$	–0.49	6.07(8)
1938.84	100	a $^2F_{5/2}$–z $^2G°_{7/2}$	–0.49	5.72(8)
2060.29	50	a $^2F_{7/2}$–z $^2F°_{7/2}$	–0.35	7.02(8)
2112.31	40	b $^2F_{7/2}$–x $^2D°_{5/2}$	–0.38	6.16(8)
2240.31	60	b $^4P_{3/2}$–z $^4P°_{5/2}$	–0.31	6.54(8)
2249.52	30	b $^4P_{5/2}$–z $^4P°_{5/2}$	–0.28	6.97(8)
2265.63	60	b $^4F_{7/2}$–z $^4D°_{7/2}$	–0.41	5.09(8)
2273.92	80	b $^4F_{3/2}$–z $^4D°_{1/2}$	–0.23	7.65(8)
2275.23	100	b $^4F_{5/2}$–z $^4D°_{3/2}$	–0.09	1.05(9)
2279.36	80	b $^4P_{1/2}$–z $^4P°_{3/2}$	–0.22	7.81(8)
2281.51	100	b $^4F_{7/2}$–z $^4D°_{5/2}$	–0.00	1.28(9)
2284.40	80	b $^2F_{7/2}$–y $^2G°_{9/2}$	–0.20	8.02(8)
2290.36	100	b $^2G_{9/2}$–x $^2F°_{7/2}$	0.28	2.40(9)
2304.78	60	b $^4F_{5/2}$–z $^2D°_{5/2}$	–0.38	5.26(8)
2309.92	50	b $^4P_{3/2}$–z $^4P°_{1/2}$	–0.38	5.15(8)
2313.30	100	b $^4F_{9/2}$–z $^4D°_{7/2}$	0.23	2.12(9)
2349.21	90	b $^4F_{3/2}$–z $^2D°_{3/2}$	–0.31	5.97(8)
2355.54	80	b $^4P_{3/2}$–y $^2F°_{5/2}$	–0.25	6.84(8)
2362.06	100	b $^4F_{7/2}$–z $^4F°_{9/2}$	–0.15	8.54(8)
2362.50	80B	b $^2D_{5/2}$–z $^4P°_{5/2}$	–0.15	8.52(8)
2372.73	100	b $^4F_{5/2}$–z $^4F°_{7/2}$	–0.19	7.65(8)
2387.41	100	b $^4F_{3/2}$–z $^4F°_{5/2}$	–0.18	7.72(8)
2388.23	80	b $^2D_{5/2}$–y $^2G°_{7/2}$	–0.18	7.81(8)
2413.94	100	b $^4F_{9/2}$–z $^4F°_{9/2}$	0.41	2.90(9)
2414.50	60	b $^4F_{7/2}$–z $^4F°_{7/2}$	0.20	1.80(9)
2417.16	2	b $^4F_{5/2}$–z $^4F°_{5/2}$	–0.33	5.39(8)
2421.91	100	b $^2G_{9/2}$–z $^2H°_{11/2}$	0.59	4.43(9)
2446.10	40	b $^4P_{1/2}$–y $^4D°_{3/2}$	–0.24	6.43(8)
2456.99	100	b $^4F_{9/2}$–z $^4G°_{11/2}$	0.62	4.56(9)
2457.24	20	b $^4F_{3/2}$–z $^4F°_{3/2}$	–0.21	6.83(8)
2468.72	80	b $^4F_{9/2}$–z $^4F°_{7/2}$	–0.34	5.01(8)
2475.87	80	b $^2D_{3/2}$–y $^2D°_{3/2}$	–0.08	8.97(8)
2486.02	50	b $^4P_{1/2}$–y $^4D°_{1/2}$	–0.34	4.97(8)

Table 7. continued.

λ (Å)[a]	Int.[a]	Transition[a]	log gf[b]	gA[b]
2488.74	60	b $^4F_{5/2}$–z $^4F^\circ_{3/2}$	–0.41	4.14(8)
2499.73	100	b $^4F_{7/2}$–z $^4G^\circ_{9/2}$	0.43	2.88(9)
2545.64	100	b $^4F_{5/2}$–z $^4G^\circ_{7/2}$	0.27	1.93(9)
2557.94	80	b $^4F_{9/2}$–z $^4G^\circ_{9/2}$	–0.20	6.43(8)
2567.44	50	b $^2D_{3/2}$–y $^4D^\circ_{5/2}$	–0.14	7.69(8)
2586.05	40	b $^4P_{5/2}$–z $^2P^\circ_{3/2}$	–0.12	7.47(8)
2593.75	60	b $^4F_{7/2}$–z $^4G^\circ_{7/2}$	–0.22	5.99(8)
2598.86	80	b $^4F_{3/2}$–z $^4G^\circ_{5/2}$	0.12	1.30(9)
2612.31	20	b $^2D_{5/2}$–y $^4D^\circ_{3/2}$	–0.37	4.20(8)
2628.67	50	b $^2G_{7/2}$–z $^2G^\circ_{7/2}$	0.21	1.57(9)
2633.17	80	b $^2G_{9/2}$–y $^2G^\circ_{9/2}$	0.41	2.44(9)
2634.15	30	b $^4F_{5/2}$–z $^4G^\circ_{5/2}$	–0.46	3.38(8)
2638.12	40bl	b $^2F_{5/2}$–z $^2G^\circ_{7/2}$	0.20	1.51(9)
2657.99	80	b $^2F_{7/2}$–z $^2G^\circ_{9/2}$	0.31	1.93(9)
2930.26	40	b $^2F_{5/2}$–z $^2D^\circ_{3/2}$	–0.39	3.15(8)
2937.71	50	b $^2F_{7/2}$–z $^2D^\circ_{5/2}$	–0.19	4.98(8)
2989.95	20	b $^2F_{5/2}$–z $^4F^\circ_{5/2}$	–0.39	3.03(8)
3001.84	80	b $^2F_{7/2}$–z $^2F^\circ_{7/2}$	0.09	9.14(8)
3034.87	10	b $^2F_{5/2}$–z $^2F^\circ_{5/2}$	–0.37	3.12(8)
3142.26	80	b $^2G_{9/2}$–z $^2G^\circ_{9/2}$	–0.37	2.86(8)

Notes. [a] From Iglesias (1955); [b] HFR + CPOL: this work. $A(B)$ is written for $A \times 10^B$; bl: blend.

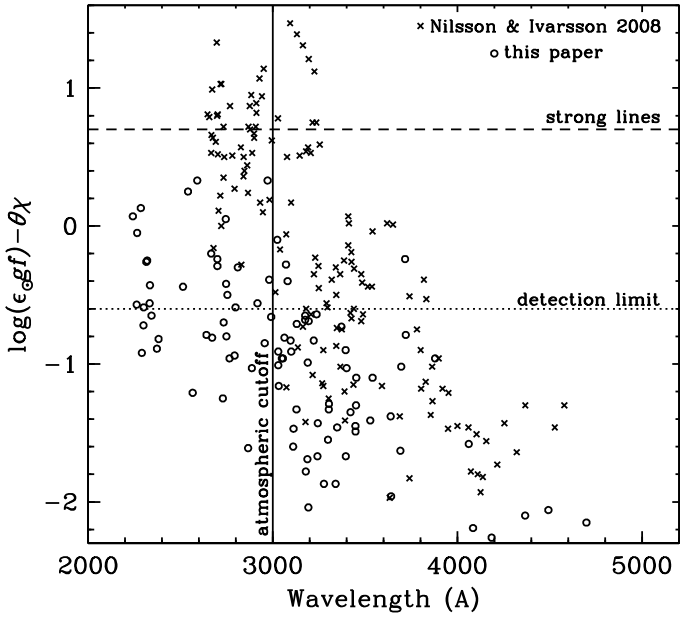

Fig. 3. Relative strengths of Nb II lines (defined as $\log \epsilon_\odot gf - \theta\chi$, see text), plotted as a function of wavelength. The atmospheric transmission cutoff wavelength is shown as a vertical line. A dotted horizontal line indicates the approximate strength for barely detectable lines in the solar spectrum, and a dashed horizontal line shows the corresponding strength for strong lines, as discussed in the text.

crowded UV domain. A good discussion of the (lack of) easily accessible Nb II lines was given by Hannaford et al. (1985).

We therefore adopted the strategy of first identifying promising transitions in one of the "*n*-capture-rich" stars known to have enhanced niobium abundances. In these stars, the contrast between Nb II line strengths and those of contaminant transitions should be at its greatest. A similar technique was applied to the analyses of Ho II (Lawler et al. 2004), Pt I (Den Hartog et al. 2005), and Tm II (Sneden et al. 2009).

For niobium, we chose CS 31082-001, the "uranium star" discovered by Cayrel et al. (2001) and discussed at length by Hill et al. (2002). Our spectrum for CS 31082-001 is described in Sneden et al. (2009). Considering all the laboratory line data in the present paper (Table 4) and in Nilsson & Ivarsson (2008), we were able to identify only seven transitions in the CS 31082-001 spectrum as promising niobium abundance indicators, which are listed in Table 8. This small number of lines occurred in spite of the order-of-magnitude overabundances of *n*-capture elements with respect to the Fe-group in CS 31082-001 and other *r*-process-rich stars. The chosen lines include two that are in common with the Nb II lines used by Hannaford et al. (1985): 3215.59 Å and 3740.72 Å.

In Fig. 4, we show four of the strongest Nb II lines in the spectra of the Sun and CS 31082-001. Inspection of this figure illustrates the difficulties mentioned above: all of the lines are weak and/or blended in both the Sun and the *n*-capture-rich giant. We discuss Fig. 4 further in the next subsection.

5.2. Niobium in the solar photosphere

In an attempt to derive a solar niobium abundance from the seven Nb II lines identified in the CS 31082-001 spectrum, we computed synthetic spectra within small wavelength intervals about each candidate transition. In assembling the required atomic and molecular lines, we began with the transitions in the Kurucz (1998)[2] database, and updated the transition probabilities, and the hyperfine and/or isotopic splits of *n*-capture lines described with literature references in Sneden et al. (2009). The Nb II transition probabilities and hyperfine structure data were taken entirely from this paper and Nilsson & Ivarsson (2008); since naturally-occurring niobium exists only as ^{93}Nb, isotopic wavelength shifts need not be considered. The line lists and the solar empirical model photosphere of Holweger & Müller (1974) were used as inputs to the current version of the stellar line analysis code MOOG (Sneden 1973)[3] to generate synthetic spectra. We adopted a microturbulent velocity of 0.8 km s^{-1}. These spectra were then compared to the solar photospheric center-of-disk spectrum of Delbouille et al. (1973)[4], after smoothing to account for solar macroturbulence and instrumental broadening (empirically determined as 1.5 km s^{-1}).

We adjusted the transition probabilities for lines in which accurate experimental values are missing, to reproduce the overall line absorption in the solar and CS 31082-001 spectra. The niobium abundance for each feature was then determined by comparing the synthetic and observed spectra. The line-by-line abundances obtained are given in Table 8. Values in parentheses are rough estimates, and included as consistency checks only. They were not used in computing the mean photospheric niobium abundance. From the four strongest Nb II lines, we derived $\langle \log \epsilon_\odot \rangle = 1.47$ ($\sigma = 0.02$).

The close agreement among the abundances deduced from the four strongest photospheric Nb II lines infers a very small formal sample standard deviation. However, this underestimates the true uncertainty, because every line is at least partially blended (Fig. 4), and continuum placement in the dense UV solar spectrum is not easy to establish. From repeated trial synthesis/observation matches, we estimate a more realistic

[2] Available at http://cfaku5.cfa.harvard.edu/
[3] Available at: http://verdi.as.utexas.edu/moog.html
[4] Available at http://bass2000.obspm.fr/solar_spect.php

Table 8. Solar and stellar niobium abundances.

λ (Å)	χ (eV)	log gf	Sun log ϵ	BD+17 3248 log ϵ	CS 22892-052 log ϵ	CS 31082-001 log ϵ	HD 115444 log ϵ	HD 221170 log ϵ
3194.975	0.326	0.120	1.50	−0.30	...	−0.48	(−0.9)	(−0.6)
3206.339	0.930	0.038	(1.7)	−0.08	...	−0.55	...	...
3215.593	0.439	−0.235	1.53	−0.23	−0.85	−0.66	−0.98	−0.82
3225.467	0.292	−0.008	(1.5)	−0.35	−0.72	−0.53	−0.95	−0.79
3540.959	1.031	−0.431	...	(−0.1)	(−0.6)	−0.50	...	...
3717.060	1.693	0.030	1.48	(−0.2)	...	−0.61	...	(−0.6)
3740.720	1.617	−0.307	1.47	(−0.2)	...	−0.55	...	(−0.5)
mean			1.49	−0.24	−0.78	−0.55	−0.96	−0.80
σ			0.02	0.12	0.09	0.06	0.02	0.02
#lines			4	4	2	7	2	2

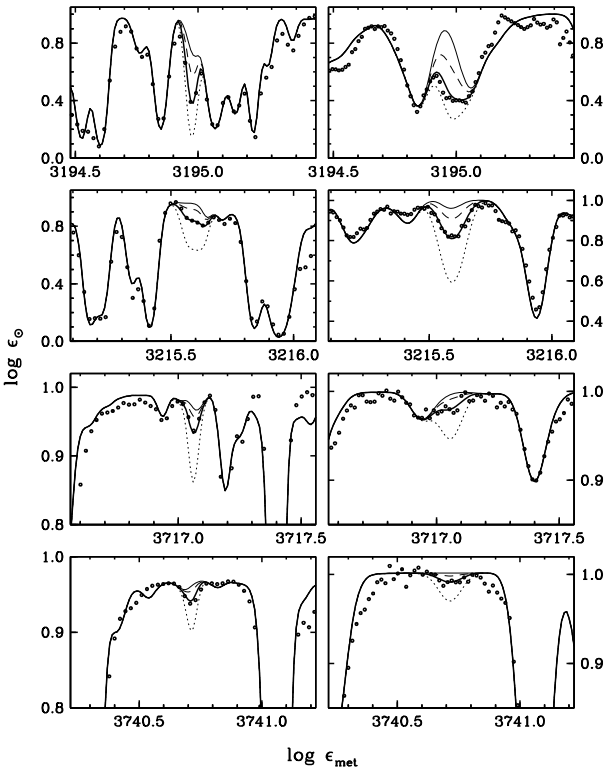

Fig. 4. Observed (points) and synthetic spectra (lines) of Nb II lines in the solar (*left-hand panels*) and CS 31082-001 (*right-hand panels*) spectra. The solar photospheric spectrum is from Delbouille et al. (1973), resampled at 0.024 Å for display purposes. The CS 31082-001 spectrum is described in Sneden et al. (2009). In each panel, the heavy black line represents the best-fit synthesis for that feature, the dotted line shows the synthesis for an increase in the Nb abundance by 0.5 dex, the dashed line shows the synthesis for a decrease by 0.5 dex, and the thin solid line shows the synthesis with no Nb contribution.

internal uncertainty for each line to be ∼±0.08, so that from four lines the standard deviation of the mean is 0.04. In Lawler et al. (2009) and references therein, we suggested that the external scale errors of solar abundances deduced from low-excitation ionized-state transitions for elements such as rare earths amount to ∼±0.03. Therefore, by combining internal and external errors we recommend adopting $\langle \log \epsilon_{\odot} \rangle = 1.47 \pm 0.06$.

Our new photospheric niobium abundance is in reasonable agreement with literature values. Hannaford et al. (1985) analyzed 11 mostly very weak Nb II lines, deriving $\langle \log \epsilon_{\odot} \rangle = 1.42 \pm 0.06$. Asplund et al. (2009) produced a new set of solar photospheric abundances, which included calculated or estimated corrections for more physically realistic 3-dimensional hydrodynamic solar models and line formation computations that account for departures from LTE. For niobium, they recommend $\langle \log \epsilon_{\odot} \rangle = 1.46 \pm 0.04$. Comparing their rare-earth $57 \leq Z \leq 72$ abundances to those published by the Wisconsin-Texas group (Sneden et al. 2009), we find $\langle \Delta \log \epsilon \rangle = -0.03$, in the sense Asplund et al. *minus* Sneden et al. This correction should apply approximately equally to niobium. If we were to adopt this small offset, then our final abundance would be $\langle \log \epsilon_{\odot} \rangle = 1.44 \pm 0.06$. Both the raw and adjusted photospheric values closely agree with abundances of chondritic meteorites, $\langle \log \epsilon_{\rm met} \rangle = 1.43 \pm 0.04$ (Lodders et al. 2009). The solar-system niobium abundance appears to be well-determined.

5.3. Niobium abundances in *r*-process-rich metal-poor giants

We used the same type of synthetic/observed spectrum matches to derive niobium abundances in 5 *r*-process-rich giants. A description of the observed spectra, model stellar atmospheres, and references to previous analyses of these stars is given by Sneden et al. (2009), and we summarize the model parameters in Table 9.

At near-UV wavelengths, the continuum opacities cease to be dominated by H^- in the spectra of cool, metal-poor giants. A large amount of the opacity originates instead from Rayleigh scattering, as emphasized by, e.g., Cayrel et al. (2004). Including this scattering opacity alters the equation of radiative transfer, since the source function cannot be approximated simply by the Planck function. The MOOG analysis code was modified to account for this more complex radiative transfer environment in which the Planck function is linked to the continuum pure absorption opacity and the mean intensity is linked to the scattering (Sobeck et al. 2009). We applied the modified code to our analysis of the Nb II lines in the *r*-process-rich giants.

In Fig. 4, we compare synthetic and observed spectra for CS 31082-001. Comparison of these with the same lines in the solar spectrum shows that derivation of reliable niobium abundances are challenging in *r*-process-rich stars in spite of their order-of-magnitude agreement between *n*-capture-element overabundances. Of the five program metal-poor stars, CS 31082-001 is the most suitable candidate for a niobium abundance study. The other four stars are challenging in one or more ways: they have poorer quality spectra (in the case of CS 22898-052), smaller *n*-capture enhancement (HD 115444), higher Fe-peak metallicity (HD 221170), or a combination of these effects. The number of transitions used for each star, rather than the formal line-to-line scatter σ, should indicate to the reader the reliability of the mean abundance.

Table 9. Stellar model parameters.

	BD+17 3248	CS 22892-052	CS 31082-001	HD 115444	HD 221170
$T_{\rm eff}$ (K)	5200	4800	4825	4800	4510
log g	1.80	1.50	1.50	1.50	1.00
[Fe/H]	−2.10	−3.12	−2.91	−2.90	−2.19
v_t (km s^{-1})	1.90	1.95	1.90	2.00	1.80
Ref.	1	2	3	4	5

References. 1: Cowan et al. (2002); 2: Sneden et al. (2003); 3: Hill et al. (2002); 4: Westin et al. (2000); 5: Ivans et al. (2006).

Previous analyses of these stars only used the strong 3215.59 Å Nb II line, and it is also the only line that we could reliably employ in all of these stars and the Sun. We therefore used this line to connect to past work in two ways. First, we repeated our synthetic spectrum calculations for this line with the assumption of a pure Planck source function. As expected, we found that the disagreements between the "scattering" and "Planck" abundances vary as a function of temperature. With $T_{\rm eff}$ = 5200 K (Table 9), BD+17 3248 is found to have essentially identical abundances with the two methods. The stars CS 22892-052, CS 31082-001, and HD 115444 have $T_{\rm eff} \simeq 4800$ K, and for these stars inclusion of scattering in the continuum source function results in abundances that are lower by ≃0.06 than those based on Planck-function calculations. However, in HD 221170, with $T_{\rm eff}$ = 4510 K, the effect is more severe: the new calculations are lower by 0.45 dex. Caution is required when interpretating our niobium abundance for this star.

We also compared our results with previously published abundances. Our value for CS 31082-001 should be the most reliable since it is based on seven transitions that yield internally consistent results (Table 8). This abundance, log ϵ(Nb) = −0.55, is identical to that of Hill et al. (2002). The new abundance for BD+17 3248 is 0.06 less than that of Cowan et al. (2002), and for CS 22892-052 it is 0.02 more than that of Sneden et al. (2003). Westin et al. (2000) did not present a niobium abundance for HD 115444. The outlier to the general agreement is HD 221170, for which our new abundance is 0.35 dex lower than that of Ivans et al. (2006). This can be understood from the difference in analytical technique described in the preceding paragraph.

Comparisons of niobium europium abundances are useful for studying the relative r- and s-process strengths. About 2/3 of the solar-system niobium content is produced by the s-process, while nearly all of the solar-system europium has an r-process origin (e.g., Simmerer et al. 2004, their Table 10). The total solar-system abundance ratio is log ϵ(Nb/Eu) ≃ 0.9 (Lodders 2003; Asplund et al. 2009; Lodders et al. 2009). The r-process only component abundance ratio is much lower, after substracting the fraction of niobium produced by the s-process: log $\epsilon(\mathrm{Nb/Eu})_{r-\mathrm{only}} \simeq 0.1$ (Simmerer et al. 2004). Adopting the Eu abundances for the r-process-rich stars studied by Sneden et al. (2009), for CS 22892-052, CS 31082-001, and HD 221170, we derive log ϵ(Nb/Eu) ≃ 0.2, in reasonable agreement with the solar-system r-only ratio. This re-emphasizes the assertions of previous authors that these stars' n-capture abundance distributions closely mimic the r-process solar-system abundances. The other two stars have significantly higher niobium abundances relative to their europium contents: log ϵ(Nb/Eu) ≃ 0.4 for BD+17 3248, and ≃0.7 for HD 115444. It is clear that another n-capture mechanism must be invoked for these stars. Whether that extra amount is produced by a slow or rapid n-capture process is unclear from the Nb/Eu ratio alone.

6. Summary

We have reported radiative parameters in Nb II and Nb III determined from a combination of theoretical and experimental approaches. New transition probabilities (gA) and oscillator strengths (log gf-values) have been obtained for 107 Nb II transitions of astrophysical interest. They have been inferred by combining experimental lifetimes and measured branching fractions. Most of the transition probabilities reported in Table 2 for Nb II, have uncertainties between 6 and 25%. In addition, a first set of theoretical results is reported for 76 Nb III transitions. The accuracy of the results has been assessed by comparing HFR+CPOL lifetime values with experimental lifetimes obtained using the TR-LIF technique. The agreement between theory and experiment in Nb II is gratifying. We propose that our results supplant those previously published in the literature, but we provide data to allow users to draw their own conclusions.

We present hyperfine components with individual oscillator strengths for the strongest NbII lines, which are important for stellar atmosphere analyses.

Application of the Nb II data to the solar spectrum yields a photospheric abundance of log $\epsilon_\odot$ = 1.44 ± 0.06 in good agreement with the meteoritic value. The niobium abundances that we have derived in r-process-rich stars are much more reliable than those reported by previous analyses.

Acknowledgements. This work was financially supported by the Integrated Initiative of Infrastructure Project LASERLAB-EUROPE, contract RII3-CT-2003-506350, the Swedish Research Council through the Linnaeus grant, the Knut and Alice Wallenberg Foundation and the Belgian FRS-FNRS. E.B., P.Q. and P.P. are, respectively, Research Director, Senior Research Associate and Research Associate of the FRS-FNRS. V.F. acknowledges a fellowship from FRIA. C.S. has been funded by US National Science Foundation grants AST-0607708 and AST-0908978. We thank Prof. S. Svanberg (Lund Laser Centre) for the hospitality enjoyed in his laboratory during the measurements. Useful discussions with S. Van Eck and A. Jorissen (Brussels) are greatly acknowledged.

References

Allen, D. M., & Porto de Mello, G. F. 2007, A&A, 474, 221
Asplund, M., Grevesse, N., Sauval, A. J., & Scott, P. 2009, ARA&A, 47, 481
Beck, D. R., & Datta, D. 1995, Phys. Rev., A52, 2436
Bergström, C. G., Faris, H., Hallstadius, G. W., et al. 1988, Z. Phys. D: At. Mol. Clusters, 8, 17
Biémont, É. 2005, Phys. Scr., T119, 55
Biémont, É., & Quinet, P. 2003, Phys. Scr., T105, 38
Cayrel, R., Hill, V., Beers, T. C., et al. 2001, Nature, 409, 691
Cayrel, R., Depagne, E., Spite, M., et al. 2004, A&A, 416, 1117
Corliss, C. H., & Bozman, W. R. 1962, Nat. Bur. Stand. (US), Monogr. 53 (Washington D.C.: US Department of Commerce)
Cowan, R. D. 1981, The Theory of Atomic Structure and Spectra (Berkeley: University of California Press)
Cowan, J. J., Sneden, C., Burles, S., et al. 2002, ApJ, 572, 861
Delbouille, L., Roland, G., & Neven, L. 1973, Atlas photométrique du spectre solaire de λ3000 a λ10 000, Liège: Université de Liège, Institut d'Astrophysique

Den Hartog, E. A., Herd, M. T., Lawler, J. E., et al. 2005, ApJ, 619, 639
Duquette, D. W., Den Hartog, E. A., & Lawler, J. E. 1986, J. Quant. Spectr. Rad. Transf., 35, 281
Eliason, A. Y. 1933, Phys. Rev., 43, 745
Fivet, V., Palmeri, P., Quinet, P., et al. 2006, Eur. Phys. J. D, 37, 29
Fivet, V., Biémont, É., Engström, L., et al. 2008, J. Phys. B: At. Mol. Opt. Phys., 41, 015702
Fraga, S., Karwowski, J., & Saxena, K. M. S. 1976, Handbook of Atomic Data (Amsterdam: Elsevier)
Garstang, R. H. 1981, PASP, Pac., 93, 641
Gayazov, R. R., Ryabtsev, A. N., & Churilov, S. S. 1998, Phys. Scr., 57, 45
Gibbs, R. C., & White, H. E. 1928, Phys. Rev., 31, 520
Hannaford, P., Lowe, R. M., Biémont, É., & Grevesse, N. 1985, A&A, 143, 447
Hill, V., Plez, B., Cayrel, R., et al. 2002, A&A, 387, 560
Holweger, H., & Müller, E. A. 1974, Sol. Phys., 39, 19
Huber, M. C. E., & Sandeman, R. J. 1986, Rep. Prog. Phys., 49, 397
Humphreys, C. J., & Meggers, W. F. 1945, J. Res. Nat. Bur. Stand., 34, 481
Iglesias, L. 1954, An. de la Real Soc. Esp. de Fis. y Quim. L (7−8), 135
Iglesias, L. 1955, J. Opt. Soc. Am., 45, 856
Ivans, I. I., Simmerer, J., Sneden, C., et al. 2006, ApJ, 645, 613
Kurucz, R. L. 1998, Fundamental Stellar Properties (Dordrecht: Kluwer), IAU Symp., 189, 217
Lawler, J. E., Sneden, C., & Cowan, J. J. 2004, ApJ, 604, 850
Lawler, J. E., Sneden, C., Cowan, J. J., Ivans, I. I., & Den Hartog, E. A. 2009, ApJS, 182, 51
Lebzelter, Th., & Hron, J. 1999, PASP, 351, 533
Lodders, K. 2003, ApJ, 591, 1220
Lodders, K., Palme, H., & Gail, H.-P. 2009, in Landolt-Börnstein, New Series, Astronomy and Astrophysics (Berlin: Springer Verlag), submitted [arXiv:0901.1149]
Lugaro, M., Herwig, F., Lattanzio, J. C., Gallino, R., & Straniero O. O. 2003, ApJ, 586, 1305
Moore, C. E. 1958, Atomic Energy Levels, Vol. III, NBS Circular 467, Washington D.C., US Department of Commerce
Moore, C. E., Minnaert, M. G. J., & Houtgast, J. 1966, The solar spectrum 2935 Å to 8770 Å, Nat. Bur. Stds. Monograph, Washington: US Government Printing Office
Nilsson, H., & Ivarsson, S., 2008, PASP, 492, 609
Palmeri, P., Quinet, P., Wyart, J.-F., & Biémont, E. 2000, Phys. Scr., 61, 323
Plez, B., Van Eck, S., Jorissen, A., et al. 2003, Modelling of Stellar Atmospheres, ed. N. E. Piskunov, W. W. Weiss, & D. F. Gray, IAU Symp., 210
Quinet, P., Palmeri, P., Biémont, É., et al. 1999, MNRAS, Soc., 307, 934
Ryabtsev, A. N., Churilov, S. S., & Litzén, U. 2000, Phys. Scr., 62, 368
Salih, S., & Lawler, J. E. 1983, Phys. Rev. A, 28, 3653
Sheriff, R. E., & Williams, D. 1951, Phys. Rev., 82, 651
Sikström, C. M., Nilsson, H., Litzén, U., Blom, A., & Lundberg, H. 2002, J. Quant. Spec. Radiat. Transf., 74, 355
Simmerer, J., Sneden, C., Cowan, J. J., et al. 2004, ApJ, 617, 1091
Sneden, C. 1973, ApJ, 184, 839
Sneden, C., Cowan, J. J., Lawler, J. E., et al. 2003, ApJ, 591, 936
Sneden, C., Lawler, J. E., Cowan, J. J., Ivans, I. I., & Den Hartog, E. A. 2009, ApJS, 182, 80
Sobeck, J. S., et al. 2009, ApJ, submitted
Van Eck, S., & Jorissen, A. 1999, A&A, 345, 127
Vanture, A. D., Smith, V. V., Lutz, J., et al. 2007, PASP, 119, 147
Wallerstein, G., & Dominy, J. F. 1988, ApJ, 330, 937
Westin, J., Sneden, C., Gustafsson, B., & Cowan, J. J. 2000, ApJ, 530, 783
Whaling, W., Carle, M. T., & Pitt, M. L. 1993, J. Quant. Spec. Radiat. Transf., 50, 7
Xu, H. L., Jiang, Z. K., Zhang, Z. G., et al. 2003, J. Phys. B: At. Mol. Opt. Phys., 36, 1771
Xu, H. L., Persson, A., Svanberg, S., et al. 2004, Phys. Rev. A, 70, 042508